Remediation experiment of Ecuadorian acid mine drainage: geochemical models of dissolved species and secondary minerals saturation.

Joaquín Delgado[1, 2], Cinta Barba-Brioso[3*], Diana Ayala [4], Tomasz Boski[2], Sandra Torres[5], Edmundo Calderón[5], Flavio López[5, 6]

[1] *Department of Physical, Chemical and Natural Environments. Faculty of Experimental Sciences. Pablo de Olavide University 41013, Seville, Spain.*

[2] *Centre for Marine and Environmental Research. Faculty of Science and Technology. Algarve University, 8005-139, Faro, Portugal. .*

[3] *Department of Crystallography, Mineralogy and Agricultural Chemistry. Faculty of Chemistry. Seville University. 41012, Seville, Spain.*

[4] *Department of Civil and Environmental Engineering. Biogeochemistry Dual Major Program. The Pennsylvania State University, 16802, PA, USA.*

[5] *National Research Institute of Geology, Mining and Metallurgy, Quito, Ecuador.*

[6] *Central University of the Ecuador, 170129, Quito, Ecuador.*

*Corresponding author: Cinta Barba-Brioso, cbarba@us.es.Telephone-fax numbers: (+34) 954556321; 954557141

ABSTRACT: Acid mine drainage is one of the main environmental hazards to ecosystems worldwide and it is directly related to mining activities. In Ecuador, such acidic-metallic waters are drained to rivers without treatment. In this research, we tested a laboratory combined (Ca-Mg) Dispersed Alkaline Substrate (DAS) system as an alternative to remediate acid drainage from the Zaruma-Portovelo gold mining site, at El Oro, Ecuador. The system worked at low and high flow hydraulic rates during a period of 8 months, without signs of saturation. . Analysis of physico-chemical parameters and water composition (ICP-OES, ICP-MS)demonstrated that treatment effectively increased water pH and promoted the retention of about 80 % of Fe, Al, Mn and Cu. Under acid conditions As, Cr and Pb concentrations decreased with Fe and possible precipitation of jarosite and schwertmannite. However, the homogeneous depletion of Cr at pH above 6 could be related to ferrihydrite or directly with $Cr(OH)_3$ precipitation. After DAS-Ca, sulphate, phosphate and rare earth elements (REE) concentrations decreased to 1912, 0.85 and 0.07 mg/L respectively, while DAS-Mg contributed to form a complex model of minor carbonate and phosphate phases as main sink of REE. DAS-Mg also promoted the retention of most divalent metals at pH values over seven. Thus, this low cost treatment could avoid environmental pollution and international conflicts. Anyway, further investigations are needed to obtain higher Zn retention values.

Keywords: Zaruma-Portovelo mining district; Hydro-geochemistry; AMD; Water remediation; Metal removal; Secondary mineral cycles; mine waste revalorization.

1. Introduction

Acid mine drainage (AMD) generated from abandoned mining activities and uncontrolled tailing dumps is a global socio-environmental concern. Acidic waters are produced from the oxidation of pyrite and other metal sulphides disposed as million tons of sulphate-rich wastes worldwide. Such wastes once exposed to oxidation under atmospheric conditions generate highly acid leachates with extreme concentrations of metal-metalloids and sulphates known as AMD (Ayala et al., 2015; Younger et al., 2002). Extended areas of streams directly affected by AMD present poor water quality incapable of sustaining a healthy macro-life (e.g., fish) (Bigham and Cravotta, 2016).

AMD mainly affects the quality of waters draining mining sites. In Ecuador, for example, mining sites located in the southern part have affected the Puyango River basin, one of the most important basins that flows to the Pacific Ocean crossing southern Ecuador and northern Peru (Betancourt et al., 2005). In its upper course, the Puyango River flows through the Zaruma-Portovelo gold mining site (Fig. 1). The climate of the area is characterised by a high variability of temperature and precipitation with a mega-thermal dry weather dominating Portovelo (mean annual temperatures of 24 ºC and precipitation oscillating between 500 and 2000 mm). Zaruma-Portovelo is located over the palaeozoic metamorphic complex of El Oro, covered by cretaceous volcanic rocks and subsequently intruded by cenozoic igneous complexes. The ore at this site consist mainly of gold and silver, included in quartz veins associated to sulfides aspyrite, chalcopyrite, galena, sphalerite (PRODEMINCA, 1999). Metallurgical processing plants implies a variety of methods for precious metal recovery from ore extracted within and outside the Zaruma-Portovelo district. Such variability of ore sources and ore processing methods have led to the release of Fe, Cu, Pb, Zn, As, Cd, and Bi from geochemically heterogeneous tailings, harder to dispose and difficult to monitor (Delgado et al., 2018). Around 87 to 110 small-scale active processing plants (Fig. 1) in the Zaruma-Portovelo mining site (Pazmiño, 2013) store tailings in dams located at the river edges or release them directly to the river. A potential product from the oxidation of such tailings is AMD. Recent studies demonstrated how mining activities impacted negatively on Amarillo River and the Calera River, effluents of the Puyango watershed (Tarras-Wahlberg et al. 2001; Tarras-Wahlerberg and Lane, 2003; Guimarães et al., 2011; Ayala and López, 2014).

In 2008, considering the Binational Convention Puyango-Tumbes (1971), the Republic of Peru promoted an international claim against Ecuador, due to the extreme pollution detected in the lower part of Puyango watershed. Since then, Ecuadorian government has promoted continuous efforts to address this situation.

However, wider knowledge on the toxic elements cycles and development of novel techniques for environmental remediation are necessary to implement a correct basin management.

In this sense, several remediation strategies have been designed to reduce the environmental impact of mine tailings around the wold. One option is the application of active treatments consisting of controlled addition of chemicals into the acidic discharge and/or wastes to increase pH and decrease metals mobility. However, active treatments are expensive (Skousen et al., 1990), impracticable at abandoned sites, and generate products even harder to dispose. On the other hand, passive treatment systems (PTS) do not need continuous addition of reagents and require occasional maintenance, becoming an economic option for AMD remediation. Typical AMD treatment systems tends to lose reactivity or permeability due to the formation of precipitates coating the limestone grains or filling the pore space of the system (Simon et al., 2005; Pérez-López et al. 2007). To address these problems, Rötting, Thomas, Ayora and Carrera (2008) developed the Dispersed Alkaline Substrate (DAS), which consists of a reactive mixture of wood shavings and limestone sand. The high metal removal performance of this reactive mixture has been tested both in laboratory columns (Rötting, Thomas et al., 2008) and field-scale experiments (Rötting, Caraballo, Serrano, Ayora and Carrera, 2008; Caraballo, Rötting, Nieto and Ayora, 2009). Nevertheless, DAS could be insufficient to remediate high concentrations of divalent metals such as Zn, Mn, Ni or Cd (Rötting, Ayora and Carrera, 2008) since: (i) under field conditions, calcite dissolution only raises pH values around 7, insufficient to precipitate divalent metals (Cortina et al., 2003). (ii) At extremely high concentrations, metals could be toxic to sulphate reducing bacteria, responsible for inducing precipitation of metal-sulphides (Cabrera et al., 2006). (iii) Sorption and exchange sites may be rapidly saturated under high metal loads (Gibert et al., 2005).

Rötting et al. (2006) conducted laboratory column experiments that demonstrated that caustic magnesia (MgO) could be used to remove high concentrations of divalent metals from solution. Reactivity of MgO was improved when mixed with quartz sand or wood fragments, which favoured the creation of a more reactive and permeable substrate. In fact, a combined DAS (Ca-Mg) created a more reactive substrate system with a higher-porosity matrix and a large surface area that accelerated reaction kinetics and enhanced its permeability, two great advantages for a passive AMD treatment system such as DAS.

This technology has been successfully applied at sites with moderate-high acidity and metal concentrations under humid climate (i.e. Rötting et al., 2006; Rötting, Ayora and Carrera, 2008; Rötting, Caraballo, et al. 2008; Rötting, Thomas et al., 2008; Caraballo, Rötting, Macías, Nieto and Ayora 2009; Caraballo, Rötting,

Nieto et al. 2009, Caraballo et al. 2011; Macías et al., 2012). However, the effectiveness of the passive treatment (DAS-type) has not been tested in dry-megathermic climate conditions or AMD generated from tailings generated in the Zaruma-Portovelo mining district.

On the other hand, Rare Earth Elements (REE) have been frequently used as environmental tracers because they help us to estimate the affection degree of polluted sites by mining activities (i.e., Olías et al., 2005; López-González et al., 2012; Delgado et al., 2012). In addition, REE (especially Eu, Tm, Lu and Y) are now widely used in several technologies, from clean energy tomilitary systems (Zhou et al., 2016). This trend will lead to a continuous increase in demand for REE in the coming decades (Alonso et al., 2012), which will be traduced in a higher request for global production of REE. Normally, REE are associated with Ca, Th and U, so their appearance is not consistent with the demand for individual elements. This poses restrictions on the survey of REE projects (Zhou et al., 2017). For this reason, recent studies are lending special interest in their behaviour under acidic environments condition (e.g. Ayora et al., 2016; Macias et al., 2017) and focusing their effort to determine the degree of REE recuperation from AMD treatment systems, providing added value to the process by reusing the waste. REE concentration in waters decreases as pH increase, which is usually the result of simultaneous processes as sorption to suspended particles (Gammons et al., 2005), coprecipitation with Al-and Fe- oxyhydroxides and the complexation with humic substances flocculants (Åström et al., 2012). This pH dependence has been observed by analyzing AMD neutralization processes at both laboratory (Verplanck et al., 2004) and basin scales (Delgado et al., 2012), concluding that there exists a preferential HREE (heavy rare earth) partition over LREE (light) in the solid phase as pH increases above 6. Nevertheless, few studies aboard REE fractionation at alkaline conditions, suggesting that carbonates (Ayora et al., 2016) and phosphates (Delgado et al., 2012) exert a certain control in the processes of fractionation of REE at the end of the series.

Therefore, the aims of the present study were: 1) to test the effectiveness of a combined DAS (Ca-Mg) reactive substrate system to decontaminate AMD, by monitoring hydrogeochemical and thermo-hydraulic conditions at laboratory scale. 2) To set design guidelines for a future pilot-field scale implementation, based on the laboratory efficiency results under the existing climate conditions (dry-megathermic climate). 3) To gain a better understanding of REE cycles in environmental systems affected by AMD production through the study of the fractionation between aqueous and solid phases, that could be used in future studies of waste reusing.

2. Materials and methods

2.1. Experimental design – Laboratory Columns

A combined DAS (Ca-Mg) reactive substrate system to treat AMD (Rötting, Ayora and Carrera, 2008; Rötting, Thomas et al., 2008) was implemented at the National Research Institute of Geology, Mining and Metallurgy (INIGEMM) laboratories in Quito-Ecuador, as shown in Fig. 2a, 2a'. The matrix of the DAS-Ca column was composed of 25% (v/v) of 94% purity $CaCO_3$ sand (0.1–2 mm grain size) and 75% (v/v) wood chips (thickness up to 1 mm, 0.5 mm mean grain size). The matrix of the Das-Mg column was a mixture of 12.5% (v/v) commercial reactive magnesium oxide (MgO) dust (0.15 mm median particle size) and 87.5% (v/v) wood chips. The column bottoms were filled with local quartz gravels (3–5 mm diameter).

AMD collected from two sources (section 2.2) was stored under laboratory conditions in plastic containers to create a *Natural Fe-Oxidizing Lagoon* (**NFOL**) where part of the Fe(II) is biotically and abiotically oxidized and hence removed from solution (Macías et al., 2012). A peristaltic pump (LongerPump® BT100-1 L) pumped the partially treated effluent to the DAS-Ca column, from which it flowed to the DAS-Mg column. The experience was conducted in duplicate (Fig. 2a).

To start the experiment, both columns were slowly saturated with AMD and a permanent level of solution was maintained as a supernatant (see Fig. 2b). The system performed a low flow rate period (7 months) and a high flow rate period (4 weeks) to test the efficiency of the columns with different hydraulic residence times. Assuming a mean porosity of 50%, (Rotting, Ayora and Carrera, 2008) and Darcy constant velocities of 0.8 ml/min and 1.4 ml/min, the mean flow rates were 0.096 m^3/m^2d (0.66 L/day, with 8 days residence time) and 0.21 m^3/m^2d (1.44 L/day, assuming 3 days residence time) for low and high flow rate, respectively.

2.2. Field water analysis and monitoring

Two AMD-sources located in the Zaruma-Portovelo mining site (ZPMS) were selected for water samples collection (Fig. 1). The first point, A*MD-Buza* consisted on a leachate derived from environmental liabilities (located near the confluence of Amarillo and Calera rivers). The strong seasonality (hot-dry climate conditions) and lack of rain over a long period produced the drying of this creek. Therefore, the AMD sampling site changed to the nearby *AMD-Torata* mine shaft, characterized by a permanent flow.

This change allowed us simulating the response of the combined DAS (Ca-Mg) reactive to variable hydrochemical characteristics of input acid leachates derived from geochemically heterogeneous tailings (Delgado et al., 2018).

During the experiment, the system was working at open laboratory conditions (environmental variation of temperature). Climatic data were obtained from INANHI (National Institute of Meteorology and Hydrology) for inter-annual treatment period. Water samples along the columns were collected from the sampling ports showed in Fig. 2b. The inflow container (AMD-Input; #1), supernatant water (Supra-; #2 and #7), drain pipe (Out-#6 and #11), and Output container (Out-Final; #12) were sampling every 15 days. Samples from the intermediate sampling ports located in the reactive zones (#3, 4, 5, 8, 9 and 10) were taken monthly.

Physico-chemical parameters pH, electrical conductivity (E.C.), redox potential (Eh), dissolved oxygen (D.O.) and temperature (T) were measured using a multi-parameter sensor (HANNA HI9828). Major cations and trace elements were measured in filtered water samples (0.2 μm) by inductively coupled plasma–atomic emission spectroscopy (ICP-OES, model Optima 8300, Perkin Elmer, detection limits in Table 1). REE were determined by inductively coupled plasma–mass spectroscopy (ICP-MS, model Agilent 7500ce). Dissolved sulphate (SO_4^{2-}) and phosphate (PO_4^{3-}) were determined by UV-Vis spectrometry using a HACH DR6000 spectrophotometer with 10 mL quartz cells. Sulphate analysis was based on a turbidimetric method 4500-SO_4^{2-}E methodology with barium chloride (APHA, 2012a). Phosphate was quantified following the APHA method 4500-PE and adapted with a standard addition technique to eliminate the arsenate interference (APHA, 2012b).

Certified ICP Multi-Element standard solutions from AccuStandard, SQS-01-1CRM and SQS-02-R1-1CRM according to the EPA 200.7 and EPA 6010 Series, were used for calibration and accuracy control. Additionally, certified reference material for Effluents/Inorganic/Metal (nº1244) and inter-laboratory test for Trace Metals (Water Pollution/Trace Metals nº586) (CRM-European environmental production) are also measured as internal periodic laboratory control. Beside, nine replicates (one for each sampled matrix) were analysed to check the quality of the analysis whose relative percentage difference (% RPD) revealed low mean values for Al, Fe, Mn, SO_4^{2-} (<5%) and for Mg, Co, Ni, Pb, Zn, Cu (<10%) and acceptable values for As, Cd, Cr (<18%). Total alkalinity was measured using CHEMetrics "*Titrets*" test kits (range 10-100 or 100-1000 mg/L as $CaCO_3$, with 5% accuracy). Hydraulic conductivity *K* (cm/s) was calculated using Darcy's Law to track the reactivity of the system (Equation 1), where Q (ml/s) is flow rate, A (cm^2) is the

tank cross-section area perpendicular to flow, and L and Δh (cm) are distances and head-loss between control surfaces, respectively.

$$K = QL/A\,\Delta h \quad [1]$$

Net acidity (mg/L as $CaCO_3$ equivalents) was calculated according to Kirby and Cravotta (2005) (Equation 2), where C_X are molar concentrations (mol/L) and alk is measured as total alkalinity (mg/L as $CaCO_3$ equivalents).

$$\text{Net acidity} = 50{,}045 \times (3c_{Al} + 2c_{Fe} + 2c_{Mn} + 2C_{Zn} + 10^{-pH}) - alk \quad [2]$$

Absolute net acidity elimination and relative metal removal (r), where C_{sup} is AMD-Input concentration (mg/L) and C_{out} is Out-Final concentration (mg/L), were also calculated (Equation 3 and 4, respectively).

$$\text{Net acidity elimination} = \text{Supernatant net acidity} - \text{Drain pipe net acidity} \quad [3]$$

$$r = (C_{sup} - C_{out}/C_{sup}) \times 100 \quad [4]$$

2.3. Geochemical Modelling of major ions, trace elements and rare earth elements.

Activity and chemical speciation of dissolved species (AS, aqueous species) and the saturation indexes (SI, Equation 5) of minerals in solution present in the two columns (DAS-Ca and DAS-Mg) of the system at the end of the treatment (Torata last sampling, 20/02/2015), were calculated using *PHREEQC* modelling (version 3.1.7; Parkhurst and Appelo, 1999). The thermodynamic database of *PHREEQC* was enlarged with data from geochemical code *WATEQ4F* (Ball and Nordstrom, 1991). Solubility constants (*KS*) for schwertmannite were extracted from literature (Bigham et al., 1996) and SI were obtained following the detailed methodology described in Delgado et al., (2009).

$$SI = \log (IAP/KS) \quad [5]$$

Where SI the saturation index, IAP the ion activity product, and KS the solubility constant.

REE concentrations were normalized to the upper crust using the North-American Shale Composite (NASC) values. Finally, partition processes of the main lanthanides aqueous species from the AMD Out-Final solution were established using *CHEAQS-Next* modelling (Verweij, 2007) with stability constants of the REE sulphates complexes from NIST compilation (Martell et al., 2004).

2.4. Middle REE enrichment.

The enrichment/depletion in middle REE (MREE) gives upward concave (V-type) and convex (Λ-type) quantifiable patterns according to the traditional NASC-normalized $(La/Gd)_{NASC}$ ratio. However, using a single rare earth as representative of a set could hamper the interpretation of REE patterns in the case of exclusive fractionation affecting only that rare earth. Therefore, it would be crucial to assess the significance of the curvature effect in the MREE whole segment (Pérez-López et al., 2010). For this reason, we have calculated the index $\mathbf{E_{MREE}}$ (Enrichment of middle REE) to quantify this effect as the normalized maximum vertical difference between the polynomial curve fitting of the MREE region and its theoretical Y-axis position in the absence of enrichment or depletion (see details of the calculation method in Pérez-López et al. (2010) and Delgado et al. (2012). $E_{MREE} < 0$ and $E_{MREE} > 0$ represent depletion (concave pattern) and enrichment (convex pattern) in MREE, respectively, and thus around zero the flat patterns. The quality of the fit, and hence the significance of the curve formed by data points, was quantified by the squared correlation coefficient, R^2.

3. Results and Discussion

3.1. Hydrochemical evaluation of the combined DAS system to treat Ecuadorian mine waters.

The combined DAS (Ca-Mg) reactive substrate system was constantly monitored (Table 1). The control points appear numbered in Fig.2b. The pH of AMD-Input (#1) and Supra-Ca (#2) solutions had mean values from 2.7 to 2.4 and 4.1 to 2.3, respectively and values of E.C. characteristic of high-mineralized waters, subjected to moderate or high Ecuadorian restrictions for use in crops (MAE, 2000). After the DAS-Ca, an increase in water pH (up to 6.2), alkalinity (up to 263 mg/L) and Ca concentrations (up to 1128 mg/L), as well as a decrease in acidity, took place due to limestone dissolution (Fig. 3a, b). This process induced the removal of Fe and Al (Fig. 3c, d) and the adsorption-coprecipitation of As, Cr and Pb even at low concentrations (Fig. 3e, f).

The decrease in concentration of Al and sulphates (Fig. 3a, b) during the early stages of the treatment, led to a subsequent protons removal, pH increase and could be related with Cu removal (Fig.3c) by coprecipitation processes (Hammarstrom et al., 2005). On the other hand, the circum-neutral conditions observed in the DAS-Ca was not enough for divalent metal hydroxides to form (Cortina et al., 2003). At the supernatant of DAS-Mg (Supra-Mg #7) pH increased up to 6.7, related with the dissolution of reactive

magnesia (Mg concentrations changes from 212 to 699 mg/L) and also with the long retention time which improved retention of Fe and Al as acidity decreased. Water samples at the contact with MgO presented Al contents below 0.16 mg/L and Fe contents below 0.13 mg/L (Table 1). This almost absence of trivalent elements has been exposed as the best scenario to guarantee an optimal performance of the MgO in the subsequent steps of the treatment (Caraballo, Rötting, Macías et al., 2009). After the percolation through the Mg column, Cd, Co and Ni concentrations decreased down to 0.01 mg/L, Mn decreased down to 1.71 mg/L, and Zn decreased down to 1.05 mg/L, which was directly related to the increase of Mg concentration and pH (Fig. 3a, b). According to Baes and Mesmer (1976), the more effective retention of divalent metals by hydroxides should be achieved when pH is between 8 and 10. Finally, the preservation of the waters in an Output container enabled their stability by equilibrium with atmospheric CO_2, reducing even more the trace element concentrations and pH (Table 1, Out-Final #12).

The combined DAS (Ca-Mg) reactive substrate system performed effectively. The acidity of the tested AMD waters was suppressed (Fig. 4a), even achieving negatives values (indicative of net alkaline waters). Similar results were also obtained by Rötting, Thomas et al. (2008) and Macias et al. (2012) for equivalent treatments. Similar patterns were depicted by Al (Fig. 4b), total Fe (Fig. 4c) and Zn (Fig. 4d), which across the columns and along time were progressively removed from solution without signs of reactive saturation.

3.2. Hydrogeochemical Modelling

3.2.1. Aqueous solution species and solid-phases saturation index

3.2.1.1. Iron speciation

Iron was depleted from solution in the DAS-Ca column (Table 2, Fig. 5a) probably as low-crystalline oxyhydroxydes or oxy-hydroxysulfates. According to the hydrochemical model, the soluble Fe species before Mid2-Ca (#4) were $FeSO_4^+$ (73%) and $Fe(SO_4)_2^-$ (14%). Minor proportion of Fe(III), Fe(II), $FeOH^{+2}$, $Fe(OH)_2^+$ and $FeHPO_4^+$ (3%) appeared at the contact with the Ca-column (#2 or Supra-Ca). Di-sulphate species, representative in AMD, at high SO_4^{2-} concentration (> 150 mg/L), were removed from solution, increasing the proportion of hydrolysed species (Shum and Lavkullich, 1998). In such conditions, precipitation of saturated Fe phases, H- jarosite [$(H_3O)Fe_3(SO_4)_2(OH)_6$], K-jarosite [$KFe_3(SO_4)_2(OH)_6$], schwertmannite [$Fe_8O_8(OH)_6(SO_4)$], ferrihydrite [$Fe(OH)_3$], hematite [α-Fe_2O_3], goethite [α-FeOOH],

lepidocrocite [γ-FeOOH] and maghemite [γ-Fe_2O_3], could have occurred along the DAS-Ca column (Fig. 5a).

As can be seen in Fig. 2a', the progressive increase of pH favors the formation of an " *ochre*" horizon in the first centimeters, followed of a "*white*" horizon, which probably correspond to Fe and Al precipitates, respectively, also described by Rötting et al. (2008). In this sense, according the data model H-jarosite and K-jarosite were saturated at acidic pH values (before Mid1-Ca #3, mean values SI =5.60 and 6.66, respectively), so are likely to be present, although the distinction between both phases is difficult (Sánchez-España et al., 2016). Only Mid2-Ca #4 solutions (pH = 5.8) were supersaturated in schwertmannite (Fig. 5b, SI = 7.37), the most common mineral associated to ochre precipitates at slightly acidic pH, whose saturation is controlled by [Fe^{3+}] activity (Yu et al., 1999). When solution became neutral (*Mid2-Ca* #4, pH>6), ferrihydrite probably started playing a role in metal retention. Likewise, hematite, goethite, lepidocrocite and maghemite showed positive saturation index at practically all control points (Fig. 5a). However, goethite and hematite do not usually appear as direct precipitates from AMD, due to their precipitation kinetics, but they are formed by transformation of Fe oxyhydroxide-sulphates (Acero et al., 2006; Marescotti et al., 2012). Similarly, maghemite can also be formed through dehydration and transformation of lepidocrocite and ferrihydrite, the main initial products of the oxidation and precipitation of ferrous iron bearing solutions, which can be formed at surficial temperatures (Schwertmann and Fitzpatrick 1992). After Out-Ca (#6; pH = 6.2), Fe was removed from solution.

3.2.1.2. Aluminium speciation

According to Macías et al. (2012), aluminium could be trapped as hydroxysulfates in the white precipitates shown in Fig. 2a', which could also contain gypsum. The most abundant Al aqueous species in the AMD-Input #1 were associated with sulphate compounds [$AlSO_4^+$, $Al(SO_4)_2^-$], which were replaced by hydroxylated species along the DAS-Ca column [$AlOH^{2+}$, $Al(OH)_2^+$]. Mid2-Ca (#4; pH = 5.8). Precipitation of Al species (Fig. 5b) such as alunite [$KAl_3(SO_4)_2(OH)_6$], basaluminite [$Al_4(SO_4)(OH)_{10}\cdot 5(H_2O)$], jurbanite [$Al(SO_4)(OH)\cdot 5(H_2O)$] and Al-hydroxides [$Al(OH)_{3(am)}$, gibbsite $AlOH_3$, boehmite AlO(OH) and diaspore AlO(OH)] would be significant as pH increases (Nordstrom and Alpers, 1999). Our results point that alunite (SI = 13) and basaluminite (SI = 14) could have exercised the main control of Al solubility (Fig. 5b). Sánchez-España et al. (2005) suggested basaluminite as the most probably Al phase precipitating at a range of pH between 3.3 and 5.7, although its solubility is largely

294 influenced by adsorption-coprecipitation with Fe-rich sulphates (Sánchez-España et al., 2016). After Mid3-
295 Ca (#5; pH = 6.4), Al was removed from solution.

296 3.2.1.3. Trace element partition

297 Trace element partition from solution to secondary Fe-Al solid phases is associated to adsorption and/or
298 coprecipitation processes. Mineralogical studies of ochreous-precipitates in acid environments suggest that
299 jarosite-rich (together with schwertmannite-rich) precipitates contain the highest concentrations of As and
300 Cr among all the poorly crystalline oxyhydroxysulphates (Sánchez-España et al., 2016), as well as other
301 toxic elements such as Cu, Pb and Zn (Hammarstrom et al., 2005). On the other hand, ferrihydrite-rich
302 precipitates seem to be characterized by high concentrations of Pb and relatively high content of Zn and Ni
303 (Marrescotti et al., 2012). Indeed, As and Pb showed a drastic decrease in concentration associated with Fe
304 and possible precipitation of H- and K-jarosite (see graphical abstract, ocre-Fe shadow section). The
305 behaviour of Cr under acid conditions should be controlled by jarosite (Sánchez-España et al., 2016) and
306 schwertmannite (Sánchez-España and Reyes, 2019). However, the homogeneous depletion of Cr below
307 Mid2-Ca (Fig. 3c, E; pH≈6) suggested that ferrihydrite could be involved, or directly Cr(III) precipitation
308 as $Cr(OH)_3$ could have occurred.

309 No data for saturated Cu species were obtained before Mid2-Ca #4. Until that point, main species in solution
310 were Cu^{2+} and $CuSO_4$. Conditions at Mid2-Ca could have allowed the precipitation of Cu-sulphates (Fig.
311 5c) as antlerite ($Cu_3(SO_4)(OH)_4$, SI = 0.55) and brochantite ($Cu_4(SO_4)(OH)_6$, SI = 1.42), stable phases at
312 near-neutral condition (Delgado et al., 2009; Shum and Lavkullich, 1998). After the DAS-Ca column,
313 soluble species $CuCO_3$, $CuHCO_3^+$ and $CuOH^+$ appeared. Carbonate and bicarbonate aqueous species
314 rapidly disappeared after entering the DAS-Mg column, probably due to precipitation of carbonate phases
315 (Fig. 5c) such as malachite [$Cu_3(CO_3)_2(OH)_2$] and, in less extent, azurite ($SI_{Out\text{-}final}$ 1.62 and 0.61,
316 respectively) or associated with Cu-sulphates as brochantite (Carbone et al., 2013). Noticeable changes in
317 colour in the column solid and liquid due to poorly crystalline blue-green precipitate phases (Fig. 2a') could
318 support this interpretation.

319 Evolution of aqueous Zn species in the system is very close to that of copper. Zinc cation, $ZnSO_4$ and
320 $Zn(SO_4)_2^-$ were the present species before treatment. At the contact with DAS-Ca, sulphated species were
321 diminished in favour of bicarbonate ones ($ZnHCO_3^+$). At the Out-Final, $ZnCO_3$ represented 25% of aqueous
322 compounds. Only smithsonite (SI = 0.29) and monohydrate zinc carbonate ($ZnCO_3{:}1H_2O$, SI = 0.56)
323 reached oversaturation, showing that the treatment was not enough to totally remove Zn from solution.

Papassiopi et al. (2014) also reported similar results in AMD affected waters. According to Zachara et al. (1991), in calcareous environments at relatively high concentrations of divalent metals (DAS-Mg column), their aqueous concentration (including Cd, Mn and Zn) is governed by precipitation of discrete metal–carbonate phases. The hydrochemical model pointed to oversaturation of rhodochrosite [$MnCO_3$] at Out-Mg (#11) and Out-Final (#12) (SI of 0.75 and 1.51, respectively). However, according to Jensen et al. (2002), precipitation kinetics of rhodochrosite is slow. The alkaline conditions of the final treatment allowed the saturation of carbonated phases such as huntite [$CaMg_3(CO_3)_4$], calcite or dolomite, which could be involved on coprecipitation-sorption processes, affecting solubility of Zn, Mn and other trace elements. The higher efficiency of Cu and, in less extent of Zn retention, seemed to be determined by Cu/Zn-rich phases like antlerite and brochantite at Mid1-Ca (see Graphical abstract, White-Al and Green-Cu shadow). . In AMDs derived from Zn-rich source materials the processes would involve the formation of Zn-sulphates (bianchite, serpierite, goslarite, etc., not registered in Phreeqc databases), substitution of Zn/Cu in typical phases like antlerite and brochantite, or substitution of Zn/Fe and Zn/Al in different hydro-sulphates as melanterite, copiapite, dietrichite or halotrichite group (Jambor et al., 2000). The high percentages of Zn^{2+} and $ZnSO_4$ registered in solution supports these statements.

The behaviour of toxic elements could be also controlled by phosphate phases, especially after the DAS-Ca column. In fact, the most effective PO_4^{-3} depletion occurred at pH < 3, when probably strengite [$Fe(PO_4)\cdot 2(H_2O)$] precipitated. This effect could limit the presence of $MnHPO_4$ in the DAS-Mg at the first centimetres, where PO_4^{-3} was available (Fig. 5d). On the other hand, a significant uptake of Cu, Zn, Co, Ni, Cd and Mn can be noted between Supra-Mg (#7) and Mid2-Mg (#10), as other studies report (Macias et al., 2012; Rötting et al., 2006).

3.2.2. Rare earth fractionation pattern

Poorly crystalline iron oxyhydroxysulphates can act as a preferential sink of MREE by co-precipitation-adsorption processes (Bau, 1999). The weathering of the disseminate orebody in Zaruma-Portovelo is the main source of aqueous REE (and pollutants) to the catchment basin. The first control point, AMD-Input, a typical hydrogeochemical AMD environment (acidic pH, high salinity, high sulphate concentration) revealed high ΣREE concentrations (average of 754 μg/L). In addition, $(La/Gd)_{NASC}$ and $(La/Yb)_{NASC}$ presented values lower than 1 (Table 3), suggesting MREE and Heavy REE (HREE) enrichment compared to Light REE (LREE). ΣREE, sulphates and phosphates decreased to 68.6 μg/L, 1912 mg/L and 0.85 mg/L, respectively after *DAS-Ca* (especially at *Out-Ca)*. A strong correlation (R^2=0.99) exists between

sulphate/iron and REE concentrations, indicative of the precipitation of efflorescent salts and Fe-oxyhydroxysulphates coats able to remove lanthanides from solution (Bigham et al., 1996; Pérez-López et al., 2010).

On the other hand, previous studies have demonstrated that the distribution of REE in AMD often shows NASC-normalized convex patterns with an evident MREE enrichment with respect to LREE and HREE (Verplanck et al., 1999; Ferreira da Silva et al., 2009). The "Input treatment" (AMD-input and Sup-Ca) showed a noticeable MREE enrichment, typical of convex REE NASC-normalized patterns (Fig. 6) and consistent with the positive values of E_{MREE} (+0.35 ± 0.007 with R^2 = 0.99). $(La/Gd)_{NASC}$ values remained >0 along the middle section of the treatment (Out-Ca and Sup-Mg). Nevertheless, the presence of lanthanides decreased dramatically (average E_{MREE} = 0.06 ± 0.27; R^2 = 0.92) suggesting REE fractionation processes along the treatment. Finally, at the Out-Mg or "output treatment", REE concentrations fell off the detection limit and the distribution pattern depicted a sawn plot, which clearly illustrates the absence of MREE enrichment. This REE behaviour illustrates a selective fractionation process affecting REE during the treatment, which can be clarified in the subsequence section.

3.2.3. REE speciation in experimental treatment

Sulphates were the main ligands present in AMD (Table 3) and presumably controlled the REE speciation model in accordance with numerous studies in other sulphide mining districts worldwide (Olías et al., 2005; Zhao et al., 2007). REE in AMD solutions are mostly complexed forming $LnSO_4^+$ and free trivalent-REE (Ln^{3+}, referring to any lanthanide) (Gammons et al., 2005). Regarding the aqueous-speciation, REE-sulphate complexes, mainly monosulphate-complexes ($LnSO_4^+$), were the main aqueous form at the "input treatment" (63% mean) followed by $Ln(SO_4)_2^-$ species (31%) and free ionic species (Ln^{3+}, 6.3%) (Fig. 7a). These results assimilated to those of Leybourne and Johannesson (2008) and Fernández-Caliani et al. (2009) in sulphide areas, and that of Pérez-López et al. (2010) at the Iberian Pyrite Belt, which suggested that where sulphate concentrations were high (> 2000 mg/L), $Ln(SO_4)_2^-$ in solution played an important role in REE speciation processes. An important reduction in soluble $Ln(SO_4)_2^-$ species occurred at the highest decrease of SO_4^{2-} concentration which confirmed the link between SO_4^{2-} and REE concentrations (Ferreira da Silva et al., 2009). On the contrary, $LnSO_4^+$ and Ln^{3+} species remained practically unaltered in solution. In addition, REE geochemistry in AMD solutions is strongly linked to pH, and to neutralization processes. The partition among solid phases occurs at pH values between 5 and 6 (Wood et al., 2006).

385 Indeed, REE were removed from AMD at pH 6.9, whereas, at lower pHs (< 4.5), REE stayed in solution,
386 showing a conservative behaviour. In general, partition processes could have started before the Out-Ca
387 sampling point (pH 6.2) (Fig. 7b).

388 In the DAS-Ca column, formation of Fe-ochre precipitates and Al-oxyhydroxysulphates depleted REE from
389 AMD, probably due to limestone dissolution and sorption onto Fe-Al precipitates (Verplanck et al., 2004).
390 However, the analysis conducted in *Cheaqs-Next* revealed that when Fe (11.38 mg/L) and Al (1.06 mg/L)
391 were practically consumed, REE partition continued. Therefore, carbonate and phosphate species present
392 at *Out-Ca* (pH > 6, pE = 8.6 and gross-alkalinity next to 300 mg/L) could have probably enabled REE
393 partition as $Ln(CO_3)^+$, $Ln(CO_3)_2^-$ and $LnH(CO_3)^{2+}$ (mean values of 11.6, 0.94 and 0.92%, respectively).
394 After that, in *Supra-Mg*, carbonated species increased 36.0, 12.6 and 1.64%, respectively, at a time that
395 sulphate species halved in solution. However, not only CO_3^{2-} and SO_4^{2-} participated in REE partition
396 process. Saturation index computed by *Cheaqs-Next* for $LnPO_4$ was 3.9 at *Out-Ca* and 4.5 at *Supra-Mg*,
397 showing super-saturated conditions and precipitation of phosphate (PO_4^{3-}) species. PO_4^{3-} could have also
398 contributed to partition of Ce and Gd after *Out-Ca*. (Fig. 7a). Gammons et al. (2005) suggested super-
399 saturation of $LnPO_4$ and hydrous phases (Ln were mainly La, Ce, Nd and Gd), controlling the natural REE
400 attenuation in mixing acid-neutral waters.

401 In summary, a complete depletion of REE can be observed along the water progress throughout the PTS.
402 This trend is characterised by low retention (3.6%) of total REE in the first steps (*Supra-Ca*) associated to
403 Fe-oxyhydroxysulphates, an effectively REE partition (91%) associated to Al-rich solid phases in *DAS-Ca*
404 column, and REE depletion to <0.l indicating the total removal of REE in the first section of the *DAS-Mg*
405 column associated to minor lanthanide phases. While some authors (Verplanck et al., 2004; Prudêncio et
406 al., 2015) attribute REE retention mainly to ochre precipitates in abandoned mines and passive treatment
407 systems, this investigation shows a more complex partition progress in acidic waters. Moreover, these
408 results complete other REE behaviour studies during water mixing processes (Gammons et al., 2005; Wood
409 et al., 2006), and preliminary investigations from a pilot scale passive treatment system (Ayora et al., 2016).

410

411

412

413

3.4 Efficiency of treatment and legislation issues

Results of Table 1 have been compared with reference values for irrigation waters (FAO, 1985) and consumption (WHO, 2011), and with the maximum values of discharges of elements in natural water bodies adopted by the Government Ecuadorian (MAE, 2003).

pH and acidity values after treatment were in the range proposed by the FAO and WHO (6.5 to 8.5). Although sulphate retention is high compared to recent studies (Rötting, Thomas et al., 2008; Macias et al., 2012), final SO_4^{2-} concentration (1850 mg/L) was still above the established limit of 1000 mg/L (MAE, 2003). According to Cabrera et al. (2006), these systems are ineffective in eliminating large amounts of sulphate due to the high metallic load, because these metals are toxic for the establishment of bacterial communities that reduce sulphate.

A metal removal around 100% was achieved for Fe, Al and Cu, and higher than 70% for the rest of elements except Cr (~50%) and SO_4^{2-} (~25%) (Fig. 8). Therefore, the combined DAS system is suitable to treat AMD of Ecuadorian mining areas, and probably any other in the world. Comparing the element concentrations of the Out-Final water with the guideline values for toxic elements in irrigation and drinking waters (Table 1), chemical quality of the treated waters accomplished these recommendations for most elements. Some values were slightly superior to the guidelines, but only Mn and Zn concentrations clearly surpassed those limits. Taking into account that drinking waters should be subjected to a drinking treatment, an additional analysis after those treatments should define their adjustment to human consumption. However, the results have also been compared with the maximum values of element discharges in natural waterbeds, adopted by the Ecuadorian Government (MAE, 2003).

As previously discussed, the DAS-Mg columns reflected a passivation stage by the end of the experiment, which specially affected to Zn retention. By 16/09/2014, Zn retention was around 95%, and on 20/02/2015, it decreased to 43% (Table 1). The rest of divalent metals did not undergo major changes, overcoming overall effective retentions of 80%. In this case, the final concentrations of Mn and Zn surpass these referenced limits. The discharge of these waters to rivers, as well as their use for agriculture, should be preceded by additional treatments for Mn and Zn reduction.

The high metal removal can be related to the sulphate reducing conditions achieved in the DAS-Mg, which is confirmed by the negative values of net-acidity and p.e. values of the Out-Final flow (Table 2: acidity -285 mg/L as $CaCO_{3eq}$; p.e. 7.23). Passive treatments are usually not effective removing large quantities of sulphate from AMD due to the high-metallic load because metals could be toxic for sulphate reducing

444 microbial (SRM) communities (Utgikar et al., 2003; Cabrera et al., 2006). In addition, there might not have
445 been strict anaerobic conditions for SRM to thrive. The development of fermenters is also crucial to provide
446 organic acids as carbon sources to be utilized by SRM. Therefore, the addition of a final step to promote
447 the enrichment of SRM should be tested, without dismiss other system as adsorption or ion exchange
448 processes.

449 Additionally, the control of hydraulic conductivity reflected the capability of the system of working under
450 low and high flows (Fig. 9), proving the existence of an adequate permeability during long treatment
451 periods. Moreover, the effectiveness of the treatment seemed not to be controlled by the climatic conditions,
452 even if an increase of precipitation was registered (October 2014 15th and February 20th 2015).

453 Taken into account the good response of STP, the recovery of some base metals and REE have been
454 calculated and reported in the Table 4. The high concentration obtained for some metals make it possible
455 to consider the potential recovery of metals in acid system treatment, such as Al, Cu, Fe or Zn. The potential
456 possibility of recover metals in treatment of mine waters has previously been reported by other studies
457 (Smith et al., 2013), which proposed metal recovery by solubilization of the sludge from AMD treatment
458 under soft acid conditions. This possibility can be brought to this experience, since metals are finally
459 retained in poorly crystalline oxy-hydroxides and/or oxy-hydroxysulfates. Moreover, the solid-waste could
460 contain remarkable concentrations (0.11 gr during 8 month of treatment) of high-tech metals such as REE,
461 which could be also considered as valuable by-products (Macias et al., 2017). In fact, the potential metal
462 recovery of Torata flow would be 24 kg/yr. Moreover, other valuable industrial metals such as Mn (tons/yr)
463 could increase the potential value of Zaruma-Portovelo mine waste.

464

465 **5. Conclusions.**

466 The passive treatment system responded positively during the 8 months of experimentation in the
467 laboratory, removing quantities of metals even higher than previously achieved by other systems. This fact
468 justifies the implementation of the DAS at field-pilot plant for real flows.

469 The visual observation of precipitated layers shown the important role of Fe (III) on metal retention along
470 the first centimetres of the DAS-Ca column, in form of low-crystalline oxyhydroxydes mainly jarosite,
471 schwertmannite and lepidocrocite (geochemical model support this statement). Aluminium is trapped
472 deeper as hydroxysulfate, as well as gypsum. In fact, white precipitates observed also confirm this idea.

Data of the second state of treatment (DAS-Mg) suggested that carbonates (calcite-dolomite, and in lesser extent azurite-malachite) were involved on coprecipitation-sorption processes, affecting solubility of Zn, Mn and other divalent metals. Moreover, the abundance of Zn would condition the existence of Zn-sulphates. High percentages of Zn^{2+} and $ZnSO_4$ registered in solution supported these statements. In general, the experiment confirmed that DAS-Mg column contributes to a total retention of divalent metals. In addition, the behaviour of toxic elements could be also controlled by minority phosphate and carbonate phases.

Finally, since the concentration of sulphates after treatment contravenes existing local legislation, an improvement of the system that promotes sulphate remotion is necessary.

Concerning REE fractionation processes, the study confirms the traditional trend of these elements associated to sorption onto Fe-Al rich precipitates. However, REE partition continued even when Fe and Al were consumed, so the role of carbonates and phosphates was also depicted in this REE partition. Finally, a reutilization of the solid wastes obtained from the columns can be a new-fangled source of metals and REE to the current market and could significate an excellent revalorisation of the solid-wastes. For this reason, a new approach, by mean of mineralogical characterization and selective extraction, it is actually being done to test the possibility of these wastes as a secondary source of metals and REE with economic interest.

Acknowledgements

The authors acknowledge the material and human resources displayed from INIGEMM (Ecuadorian National Research Institute of Geology, Mining and Metallurgy) and CIMA (Centre for Marine and Environmental Research, Algarve University) to favour this research.

Funding

This work was supported by PROMETEO Ecuadorian program (Secretary of Superior Education, Science, Technology and Innovation) in the framework of the project "*Experiencia Piloto en la Remediación y Mitigación de la Oxidación de Sulfuros y la Generación de AMD en Relaveras del Distrito Minero de Zaruma-Portovelo*".

References

Acero P, Ayora C, Torrento C, Nieto JM (2006) The behaviour of trace elements during schwertmannite precipitation and subsequent transformation into goethite and jarosite. Geochim Cosmochim Acta 70: 4130–4139.

Alonso E, Sherman AM, Wallington TJ, Everson MP, Field FR, Roth R, Kirchain RE (2012) Evaluating rare earth element availability: A case with revolutionary demand from clean technologies. Environ Sic Technol 46: 3406-3414.

Åström ME, Österholm P, Gustafsson JP, Nystrand M, Peltola P, Nordmyr L, Boman A (2012) Attenuation of rare earth elements in a boreal estuary. Geochim Cosmochim Acta 96: 105-119

APHA, AWWA, WEF 4500-SO_4^{2-} E (2012a) Turbidimetric Method [ed] Eugene Rice, et al Standard Methods for the Examination of Water and Wastewater. 22nd Washington, DC: American Public Health Association.

APHA, AWWA, WEF 4500-P E (2012b) Ascorbic Acid Method [ed] E Rice, et al Standard Methods for the Examination of Water and Wastewater. 22nd Washington, DC: American Public Health Association.

Ayala D, Delgado J, López F, Boski T, Calderón E (2015) Preliminary evaluation of a passive treatment for mine tailings in Portovelo, El Oro, Ecuador. 27th International Applied Geochemistry Symposium. https://www.appliedgeochemists.org/images/stories/IAGS_2015/Abstracts/27th%20IAGS_Ayala%20et%20al_Passive%20treatment%20for%20mine%20tailings%20Portovelo%20Equador.pdf

Ayala D, López F (2014) Impacto de las actividades mineras por elementos potencialmente tóxicos (EPT) en la zona sur del Ecuador. IX Congreso de Ciencia y Tecnología ESPE Volume 9 pp 98-105.

Ayora C, Macías F, Torres E, Lozano A, Carrero S, Nieto JM, Pérez-López R, Férnandez-Martínez A, Castillo-Michel H (2016) Recovery of Rare Earth Elements and Yttrium from Passive-Remediation Systems of Acid Mine Drainage. Environ Sci Technol 2016 50(15): 8255-8262

Baes CF Jr, Mesmer RE (1976) The hydrolysis of cations. John Wiley and Sons ed, New York.

Ball JW, Nordstrom DK (1991) User's manual for WATEQ4F, with revised thermodynamic data base and test cases calculating speciation of major, trace and redox elements in natural waters. US Geological Survey Open- File Report, 91-183.

528 Bau M (1999) Scavenging of dissolved yttrium and rare earths by precipitating iron oxyhydroxide:
529 experimental evidence for Ce oxidation, Y-Ho fractionation, and lanthanide tetrad effect. Geochim
530 Cosmochim Acta 63: 67–77.

531 Betancourt O, Narváez A, Roulet M (2005) Small-scale gold mining in the Puyango River Basin, Southern
532 Ecuador: A Study of environmental impacts and Human exposures. EcoHealth 2: 23-332.

533 Bigham JM, Cravotta CA (2016) Acid mine drainage, in Lal, R (ed), Encyclopedia of Soil Science (3rd),
534 CRC Press, Taylor and Francis LLC, pp 6-10. http://dx doi org/10 1081/E-ESS-120001582.

535 Bigham JM, Schwertmann SJ, Traina S, Winland RL, Wolf M (1996) Schwertmannite and the chemical
536 modelling of iron in acid sulfate waters. Geochim Cosmochim Acta 60: 2111–2121.

537 Cabrera G, Pérez R, Gómez JM, Abalos A, Cantero D (2006) Toxic effects of dissolved heavy metals on
538 Desulfovibrio vulgaris and Desulfovibrio sp strains. J Hazard Mater 135: 40–46.

539 Cánovas CR, Olías M, Nieto JM, Sarmiento AM, Cerón JC (2007) Hydrogeochemical characteristics of
540 the Tinto and Odiel Rivers (SW Spain) Factors controlling metal contents. Sci Total Environ 373: 363–
541 382.

542 Caraballo MA, Rötting TS, Macías F, Nieto JM, Ayora C (2009) Field multi-step calcite and MgO passive
543 system to treat acid mine drainage with high metal concentration. Appl Geochem 24: 301–11.

544 Caraballo MA, Rötting TS, Nieto JM, Ayora C (2009) Sequential extraction and DXRD applicability to
545 poorly crystalline Fe- and Al-phase characterization from an acid mine water passive remediation
546 system. Am Mineral 94: 1029–38.

547 Caraballo MA, Macías F, Castillo J, Quispe D, Nieto J M, Ayora C (2011) Hydrochemical performance
548 and mineralogical evolution of a dispersed alkaline substrate (DAS) remediating the highly polluted acid
549 mine drainage in the full scale passive treatment of Mina Esperanza (SW, Spain). Am Mineral 96: 1270–
550 1277.

551 Carbone C, Dinelli E, Marescotti P, Gasparotto G, Lucchetti G (2013) The role of AMD secondary minerals
552 in controlling environmental pollution: Indications from bulk leaching tests. J Geochem Explor 132:
553 188–200.

554 Cortina JL, Lagreca I, De Pablo J, Cama J, Ayora C (2003) Passive in situ remediation of metal-polluted
555 water with caustic magnesia: Evidence from column experiments. Environ Sci Technol 7: 1971–1977.

556 Delgado J, Sarmiento A, Condesso De Melo M, Nieto JM (2009) Environmental impact of mining
557 activitiesin the southern sector of the Guadiana Basin (SW of the Iberian Peninsula). Water Air Soil
558 Pollut 199: 323–41.

559 Delgado J, Pérez-López R, Galván L, Nieto JM, Boski T (2012) Enrichment of rare earth elements as
560 environmental tracers of contamination by acid mine drainage in salt marshes: A new perspective. Mar
561 Pollut Bull 64: 1799–1808.

562 Delgado J, Ayala D, Páez HS (2018) Sistema de tratamiento para mejorar la calidad de aguas de drenaje de
563 pasivos ambientales mineros en la cuenca del Río Puyango (Ecuador). Geogaceta 64: 63-66. ISSN:
564 0213-683X.

565 FAO - Food and Agriculture Organization of the United Nations (1985) Irrigation and drainage paper 29,
566 rev 1. Water quality for agriculture Food and Agriculture Organization of the United Nations 1994
567 (reprint). Ayers RS and Westcot DW. Rome. ISBN: 9251022631.

568 Fernández-Caliani JC, Barba-Brioso C, De la Rosa JD (2009) Mobility and speciation of rare earth elements
569 in acid mine soils and geochemical implications for river waters in the southwestern Iberian margin.
570 Geoderma 149: 393–401.

571 Ferreira da Silva E, Bobos I, Matos JX, Patinha C, Reis AP, Cardoso-Fonseca E (2009) Mineralogy and
572 geochemistry of trace metals and REE in volcanic massive sulfide host rocks, stream sediments, stream
573 waters and acid mine drainage from the Lousal mine area (Iberian Pyrite Belt, Portugal). Appl Geochem
574 24: 383–401.

575 Gammons CH, Wood SA, Pedrozo F, Varekamp JC, Nelson BJ, Shope CL, Baffico G (2005)
576 Hydrogeochemistry and rare earth element behaviour in a volcanically acidified watershed in Patagonia,
577 Argentina. Chem Geol 222: 249– 267.

578 Gibert O, de Pablo J, Cortina JL, Ayora C (2005) Sorption studies of Zn(II) and Cu(II) onto vegetal compost
579 used on reactive mixtures for in situ treatment of acid mine drainage. Water Res 39: 827–2838.

580 Guimaraẽs JRD, Betancourt O, Rodriguez–Miranda M, Barriga R, Cueva E, Betancourt S (2011) Long-
581 range effect of cianyde on mercury methylation in a gold mining area in southern Ecuador. Sci Total
582 Environ 409: 5026-5033.

583 Hammarstrom JM, Seal II, RR, Meierb AL, Kornfeldc JM (2005) Secondary sulfate minerals associated
584 with acid drainage in the eastern US: recycling of metals and acidity in surficial environments. Chem
585 Geol 215:407– 431.

586 Jambor JL, Nordstrom DK, Alpers CN (2000) Metal-sulfate Salts from Sulfide Mineral Oxidation. Rev
587 Mineral Geochem 40:303-350.

588 Jensen DL, Boddum JK, Tjell JC, Christensen TH (2002) The solubility of rhodochrosite (MnCO3) and
589 siderite (FeCO3) in anaerobic aquatic environments. Appl Geochem 17: 503–511.

590 Kirby CS, Cravotta CA (2005) Net alkalinity and net acidity: I Theoretical considerations. Appl Geochem
591 20: 1920–1940.

592 Leybourne MI, Johannesson KH (2008) Rare earth elements (REE) and yttrium in stream waters, stream
593 sediments, and Fe–Mn oxyhydroxides: fractionation, speciation, and controls over REE+Y patterns in
594 the surface environment. Geochim Cosmochim Acta 72: 5962–5983.

595 López-González N, Borrego J, Carro B, Grande JA, De la Torre ML, Valente T (2012) Rare-earth-element
596 fractionation patterns in estuarine sediments as a consequence of acid mine drainage: A case study in
597 SW Spain. Boletín Geológico y Minero 123: 55-64.

598 Macías F, Caraballo MA, Nieto JM, Rötting TS, Ayora C (2012) Natural pretreatment and passive
599 remediation of highly polluted acid mine drainage. J Environ Manage 104: 93-100.

600 Macías F, Pérez-López R, Caraballo MA, Ayora C, Nieto JM (2017) Management strategies and
601 valorization for waste sludge from active treatment of extremely metal-polluted acid mine drainage: A
602 contribution for sustainable mining. Journal of Cleaner Production 141: 1057-1066.

603 MAE - Ministerio de Ambiente República Del Ecuador (2000). Comisión de Medio Ambiente, Higiene y
604 Recursos Naturales Registro Oficial No 74, 10/05/2000 Anexo Valores Máximos Permisibles de los
605 Indicadores de Contaminación y Parámetros de Interés Sanitario para Descargas Líquidas.

606 MAE - Ministerio de Ambiente República Del Ecuador (2003). Texto unificado de la legislación ambiental
607 secundaria (TULSMA, Libro VI) Reglamento a la Ley de Gestión ambiental para la prevención y control
608 de la contaminación ambiental MAE, Quito, pp 319.

609 Marescotti P, Carbone C, Comodi P, Frondini F, Lucchetti G (2012) Mineralogical and chemical evolution
610 of ochreous precipitates from the Libiola Fe–Cu-sulfide mine (Eastern Liguria, Italy). Appl Geochem
611 27: 577–587.

612 Martell, AE, Smith, RM, Motekaitis, R, (2004). NIST critically selected stability constants of metal
613 complexes. NIST Standard Reference Data Base 46 Version 8.0. Gaithersburg MD.

614 Nordstrom DK, Alpers CN (1999) Geochemistry of acid mine waters. In GS Plumlee, M J Logson (Eds),
615 The environmental geochemistry of mine waters 6A. Rev Econ Geol (pp 133–160). Littleton, CO:
616 Society of Economic Geology.

617 Olías M, Ceron JC, Fernández I, De la Rosa J (2005) Distribution of rare earth elements in an alluvial
618 aquifer affected by acid mine drainage: The Guadiamar aquifer (SW Spain). Environ Pollut 135 : 53–
619 64.

620 Papassiopi N, Zaharia C, Xenidis A, Adam K, Liakopoulos A, Romaidis I (2014) Assessment of
621 contaminants transport in a watershed affected by acid mine drainage, by coupling hydrological and
622 geochemical modeling tools. Miner Eng 64: 78–91.

623 Parkhurst DL, Appelo CAJ (1999) User's guide to PHREEQC (Version 2)—A computer program for
624 speciation, batch reaction, one-dimensional transport, and inverse geochemical calculations. USGS
625 water-resources investigations report: 99–4259 (pp 312) Denver: US Geological Survey.

626 Pazmiño I (2013) Tipología de las plantas de beneficio de minerales en el Distrito Minero Zaruma-
627 Portovelo, Provincia El Oro, Quito: Instituto Nacional de Investigación Geológico Minero Metalúrgico.

628 Pérez-López R, Cama J, Nieto JM, Ayora C (2007) The iron-coating role on the oxidation kinetics of a
629 pyritic sludge doped with fly ash. Geochim Cosmochim Acta 71: 1921-1934.

630 Pérez-López R, Delgado J, Nieto JM, Márquez-García B (2010) Rare earth element geochemistry of
631 sulphide weathering in the São Domingos mine area (Iberian Pyrite Belt): a proxy for fluid-rock
632 interaction and ancient mining pollution. Chem Geol 276: 29–40.

633 PRODEMINCA, (1999) Monitoreo ambiental de las áreas mineras en el sur del Ecuador 1996-1998.
634 Proyecto de Desarrollo Minero y Control Ambiental, Swedisch Environmental Systems, Quito, 154 pp.

635 Prudêncio MI, Valente T, Marques R, Sequeira-Braga MA, Pamplona J (2015) Geochemistry of rare earth
636 elements in a passive treatment system built for acid mine drainage remediation. Chemosphere 138:
637 691–700.

638 Puig-Domènech I, (2010). MEDUSA (Make Equilibrium Diagrams Using Sophisticated Algorithms)
639 Windows interface to the MS-DOS versions of INPUT, SED and PREDOM (FORTRAN programs
640 drawing chemical equilibrium diagrams) Vers. 6 Dec 2010. Royal Institute of Technology, Stockholm,
641 Sweden.

642 Rötting TS, Cama J, Ayora C, Cortina JL, De Pablo J (2006) Use of caustic magnesia to remove cadmium,
643 nickel, and cobalt from water in passive treatment systems: Column experiments. Environ Sci Techno
644 40: 6438–6443.

645 Rötting TS, Ayora C, Carrera J (2008) Improved passive treatment of high Zn and Mn concentrations using
646 caustic magnesia (MgO): particle size effects. Environ Sci Techno 2: 9370–7

647 Rötting TS, Caraballo MA, Serrano JA, Ayora C, Carrera J (2008) Field application of calcite Dispersed
648 Alkaline Substrate (calcite-DAS) for passive treatment of acid mine drainage with high Al and metal
649 concentrations. Appl Geochem 23: 1660–1674.

650 Rötting TS, Thomas RC, Ayora C, Carrera J (2008) Passive treatment of acid mine drainage with high
651 metal concentrations using dispersed alkaline substrate. J Environ Qual 37: 1741–1751.

652 Sánchez-España J, Lopez-Pamo E, Santofimia E, Aduvire O, Reyes J, Barettino D (2005) Acid mine
653 drainage in the Iberian Pyrite Belt (Odiel river watershed, Huelva, SW Spain): Geochemistry,
654 mineralogy and environmental implications. Appl Geochem 20: 1320–1356.

655 Sánchez-España J, Yusta I, Gray J, Burgos WD (2016) Geochemistry of dissolved aluminum at low pH:
656 Extent and significance of Al–Fe(III) coprecipitation below pH 4.0. Geochim Cosmochim Acta 175:
657 128–149.

Sánchez-España J, Reyes J (2019) Comparing schwertmannite and hydrobasaluminite dissolution in ammonium oxalate (ph 3.0): implications for metal speciation studies by sequential extraction. Minerals 9: 57. https://doi.org/110 3390/min9010057.

Schwertmann U, Fitzpatrick RW (1992) Iron minerals in surface environments. In: Skinner HCW and Fitzpatrick RW (eds). Biomineralization processes of iron and manganese-modern and ancient environments. Catena Verlag, 7–30.

Shum M, Lavkulich L (1998) Speciation and solubility relationships of Al, Cu and Fe in solutions associated with sulfuric acid leached mine waste rock. Environ Geol 38: 59–68.

Simon M, Martin F, Garcia I, Bouza P, Dorronsoro C, Aguilar J (2005) Interaction of limestone grains and acidic solutions from the oxidation of pyrite tailings. Environ Pollut 135: 65–72.

Skousen J, Politan K, Hilton T, Meek A (1990) Acid mine drainage treatment systems: chemicals and costs. Green Lands 20: 31-37

Smith KS, Figueroa LA, Plumlee GS (2013) Can treatment and disposal costs be reduced through metal recovery? Golden, Colorado, USA. In: Brown, A , Figueroa, L , Wolkersdorfer, C (Eds), Reliable Mine Water Technology (Vol I), Annual International Mine Water Association Conference, pp 729-735.

Tarras-Wahlberg NH, Flachier A, Lane SN, Sangfors O (2001) Environmental impacts and metal exposure of aquatic ecosystems in rivers contaminated by small scale gold mining: The Puyango river basin, southern Ecuador. Sci Total Environ 278: 239-261.

Tarras-Wahlberg NH, Lane SN (2003) Suspended sediment yield and metal contamination in a river catchment affected by El Niño events and gold mining activities: The Puyango river basin, southern Ecuador. Hydrol Process 17: 3101-3123.

Utgikar VP, Tabak HH, Haines JR, Govin R (2003) Quantification of toxic and inhibitory impact of copper and zinc on mixed cultures of sulfate-reducing bacteria. Biotechnol Bioeng 83: 306–312.

Verplanck PL, Nordstrom DK, Taylor HE (1999) Overview of rare earth element investigations in acid waters of US Geological Survey abandoned mine lands watersheds. US Geological Survey Water-Resources Investigations Report 99- 4018A, 83–92.

Verplanck PL, Nordstrom Dk, Taylor HE, Kimball BA (2004) Rare earth element partitioning between hydrous ferricoxides and acid mine water during iron oxidation. Appl Geochem 9: 1339–1354.

Verweij W, (2007). Chemical equilibria in aquatic systems—CHEAQS Pro-PC calculating program. http://home.tiscali.nl/cheaqs/index.html.

WHO - World Health organization (2011). Guidelines for drinking water quality Vol 1, 4th edition. Genove. ISBN: 9789241548151.

Wood SA, Gammons CH, Parker SR (2006) The behaviour of rare earth elements in naturally and anthropogenically acidified waters. J Alloys Compd 418: 161–165.

Younger PL, Banwart SA, Hedin RS (2002) Mine Water - Hydrology, Pollution, Remediation. Kluwer Academic Publishers, Dordrecht.

Yu JY, Heo B, Choi IK, Cho JP, Chang HW (1999) Apparent solubilities of schwertmannite and ferrihydrite in natural stream waters polluted by mine drainage. Geochim Cosmochim Acta 3: 3407–3416.

Zachara JM, Cowan CE, Resch CT (1991) Sorption of divalent metals on calcite. Geochi Cosmochim Acta 55: 1549–1562.

Zhao F, Cong Z, Sun H, Ren D (2007) The geochemistry of rare earth elements (REE) in acid mine drainage from the Sitai coal mine, Shanxi Province, North China. Int J Coal Geol 70: 184–192.

Zhou B, Li Z, Zhao Y, Zhang C, Wei Y (2016) Rare Earth Elements Supply vs. Clean Energy Technologies: New Problems to Solve. Gospod Surowcami Miner 32: 9-44.

Zhou B, Li Z, Congcong C (2017) Global potential of rare earth resources and rare earth demand from clean technologies. Minerals. https://doi.org/10 3390/min7110203.

TABLE AND FIGURE CAPTIONS

TABLES

Table 1 Hydrochemical mean results of the main steps of treatment after the first and the last month of experience, including statistics of AMD sources (Buza and Torata) and concentration restrictions for toxic elements proposed by FAO (1985), WHO (2011) and Euadorian National Government (MAE, 2003)

Table 2 Phreeqc modelling input data from sampling 20/02/2015 of Torata AMD

Table 3 CHEAQS-Next modelling input data from sampling 20/02/2015 of the treatment

Table 4 Metal retention values from laboratory experimental columns (gr) and their potential annual removal values (tons/yr) assuming a field pilot-plant to decontaminate the average outflow of 1 L/s from Torata mine shaft

FIGURES

Fig. 1 Map of Zaruma-Portovelo mining district (ZPMD) showing punctual waste-water discharges associated to metal-processing plants, environmental liabilities and ranges of polluted zones with toxic elements (Modified from Ayala and López, 2014)

Fig. 2 Passive multi-step treatment system based in the DAS concept. **a)** Photography shown the treatment during July 2014 (starting operation); **a')** Photography showing both Ca- and Mg-DAS column during monitoring before 8 mouth of treatment (February 2015, end of the operation experiment); **b)** Schematic design of system showing most important setup parameters

Fig. 3 Distribution of water master variables (mg/L) along the stages of the passive treatment **a)** Fe, Al, net acidity and pH; **b)** Ca, Mg and sulphates; **c)** Cu, Zn, Mn, Cd, As, Pb, Co, Cr and Ni after the first month of treatment (Buza AMD-Input; Fe=Fe*10), **d, e, f)** after the last month (Torata AMD-Input; Fe=Fe/5)

Fig. 4 Evolution of parameters in the preferential sampling-points of the treatment (from 15/07/2014 to 20/02/2015). The change of water source is represented by the orange (AMD_{BUZA}) or blue (AMD_{TORATA}) background of the plots. **a)** Net acidity (mg/L CaCO3 eq; **b)** Al; **c)** Fe; **d)** Zn

Fig. 5 Results of Phreeqc-software modelling obtained along several control point (Sampling Ports shown in Figure 2) of passive treatment system. Aqueous species and solid-phases saturation indexes for: **a)** Al-rich and; **b)** Fe-rich phases; **c)** Cu- and Zn-rich phases; **d)** saturation indexes of some minor phases reported by model. Other refers minor phases whose values were always below 1%

Fig. 6 NASC-normalized REE patterns for solution of the passive treatment system. Input treatment: AMD-Input + Supra-Ca; Middle treatment: Out-Ca + Supra-Mg; Output treatment: Out-Mg + Treated output. The shadowed area refers to the variability range and dash line to the mean value

Fig. 7 Results of aqueous speciation from Torata AMD last sampling. **(A)** Average ratios of REE for Ln^{3+} aqueous species (where Ln = Lanthanides except Ce and Gd plotted separately). **(B)** Comparison between variation of the relative abundance of La^{3+} in AMD of the Iberian Pyrite Belt (Ayora et al., 2016, Figure 2) and Ln^{3+} species obtained in this study from AMD of ZPMD, showing the evolution based on pH and the different section of treatment control. Thermodynamic data from MEDUSA database (Puig-Domenech, 2010)

Fig. 8 Boxplot showing the degree of efficiency of total treatment time as metal removal percentage between input-AMD (laboratory) and output container

749 **Fig. 9** Trend of hydraulic conductivity (K) during the treatment showing the high flow period (4 weeks)
750 and inter-annual (2014-2015) mean climate range (source INAMHI, Nacional Institute of Meteorology and
751 Hydrology) to test the efficiency of the columns with different residence times and metal concentration
752 input

GRAPH ABSTRACT

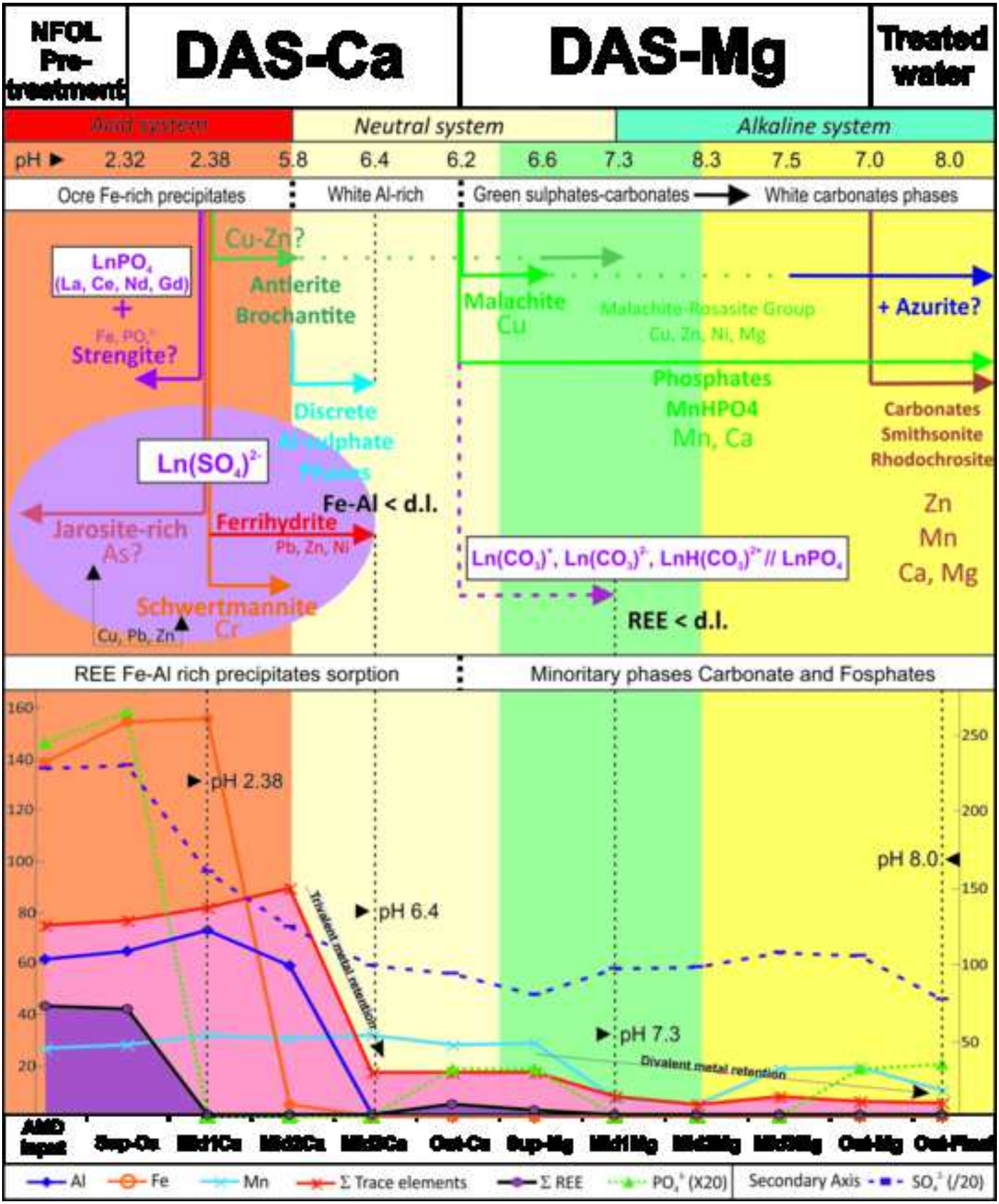

Figure 1

Click here to access/download;Figure;Figure 1.tif

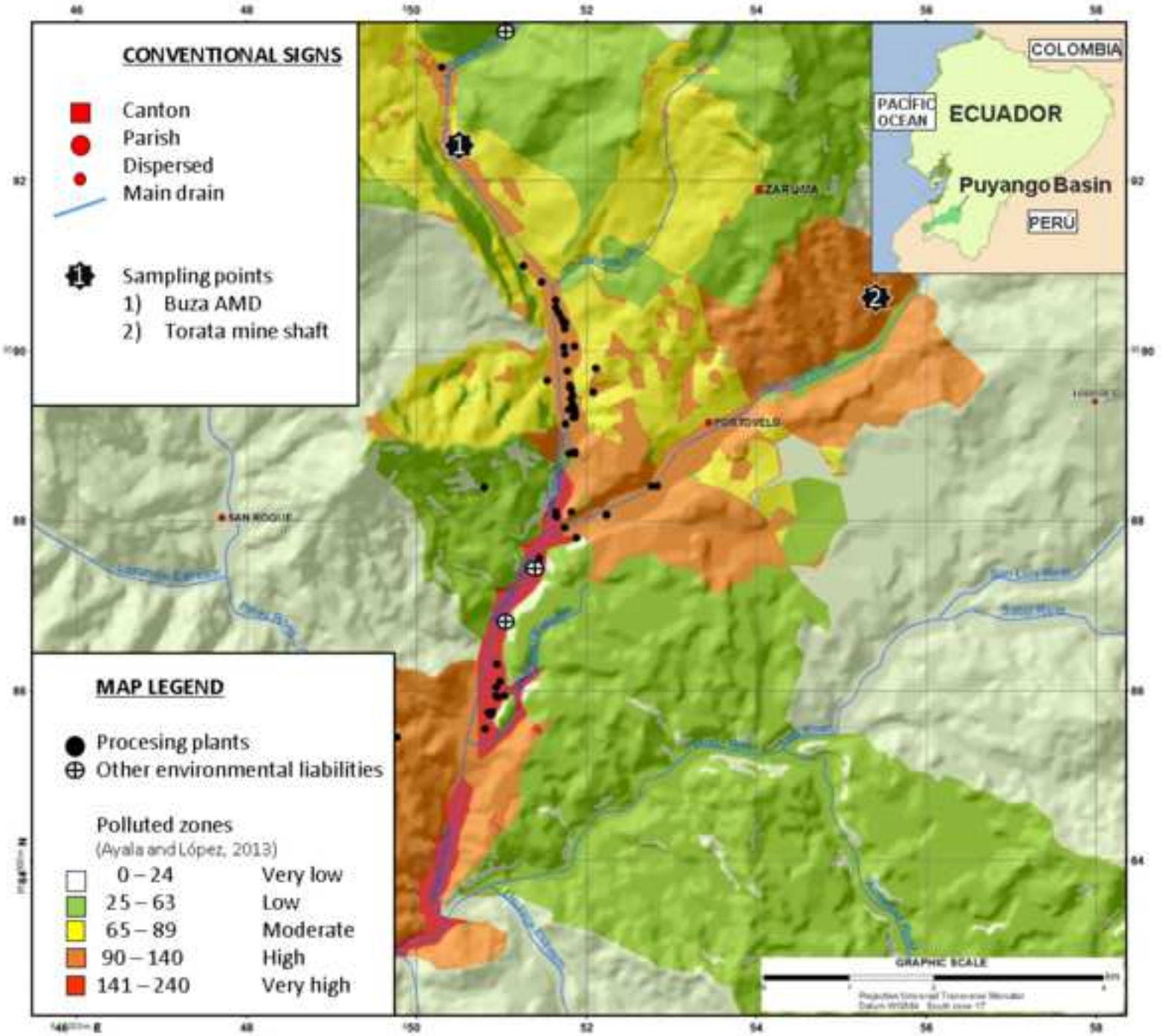

Figure 2-revised

Click here to access/download;Figure;Figure 2.tif

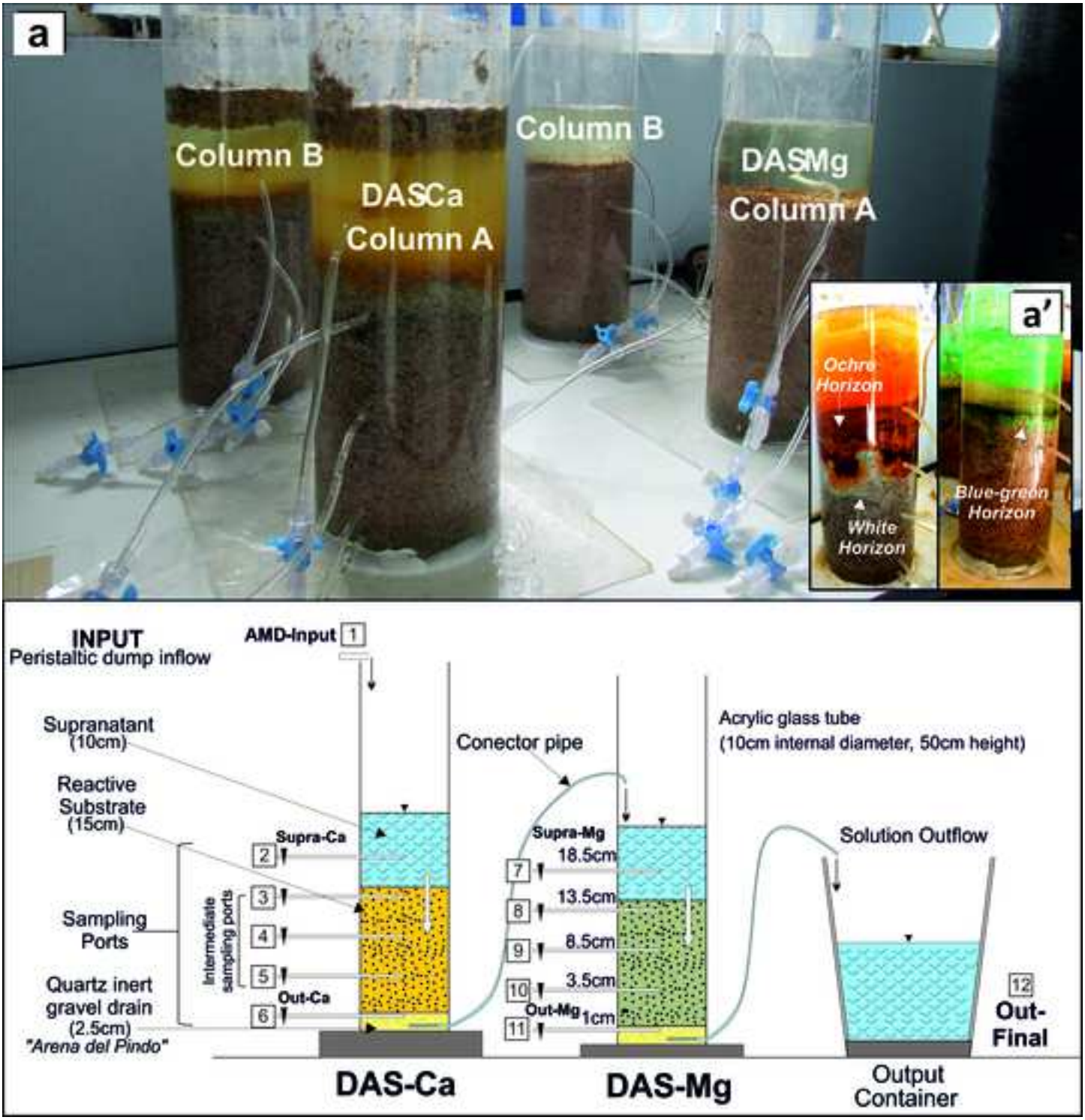

Figure 3

Click here to access/download;Figure;Figure 3.tif

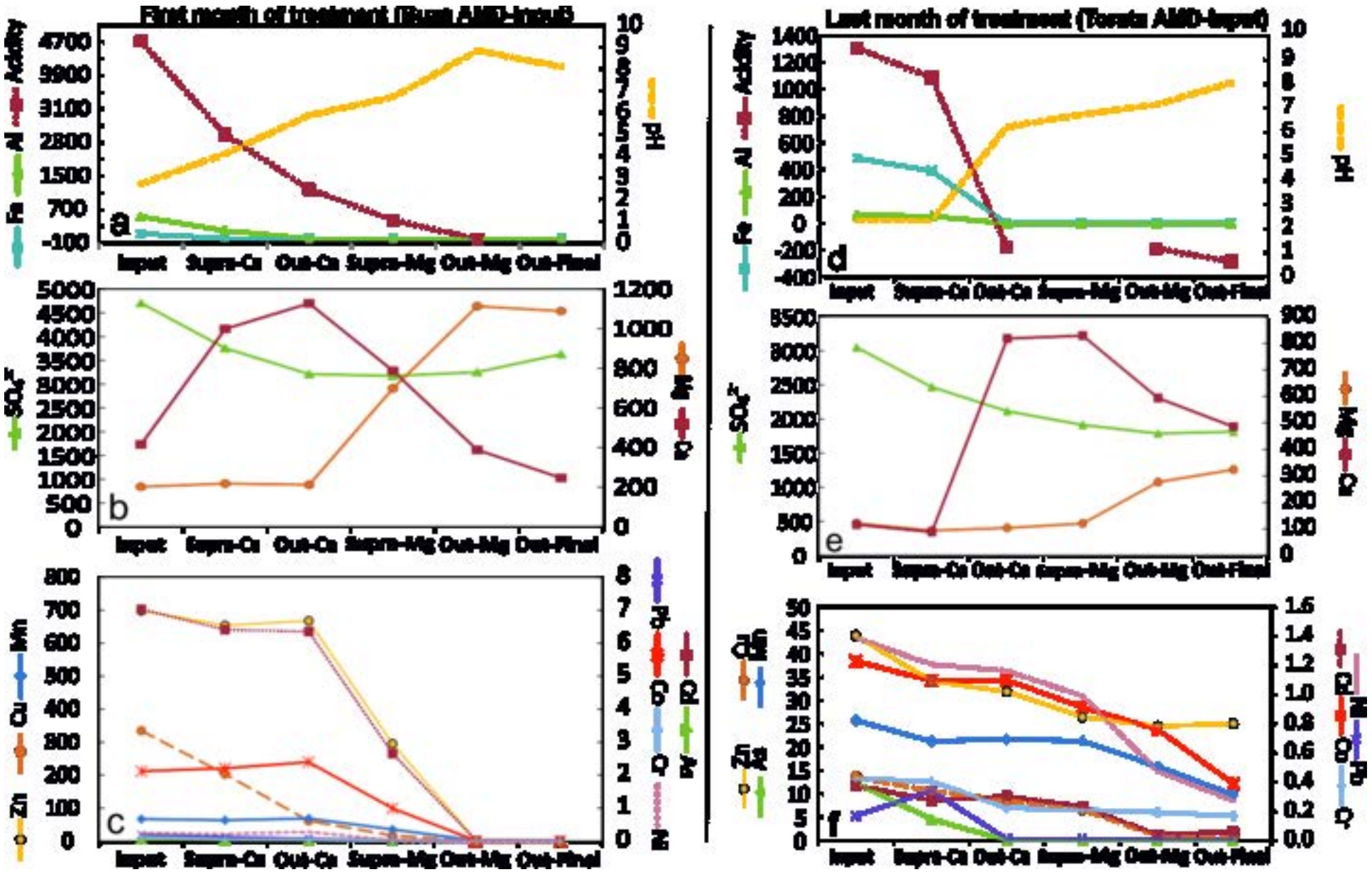

Figure 4

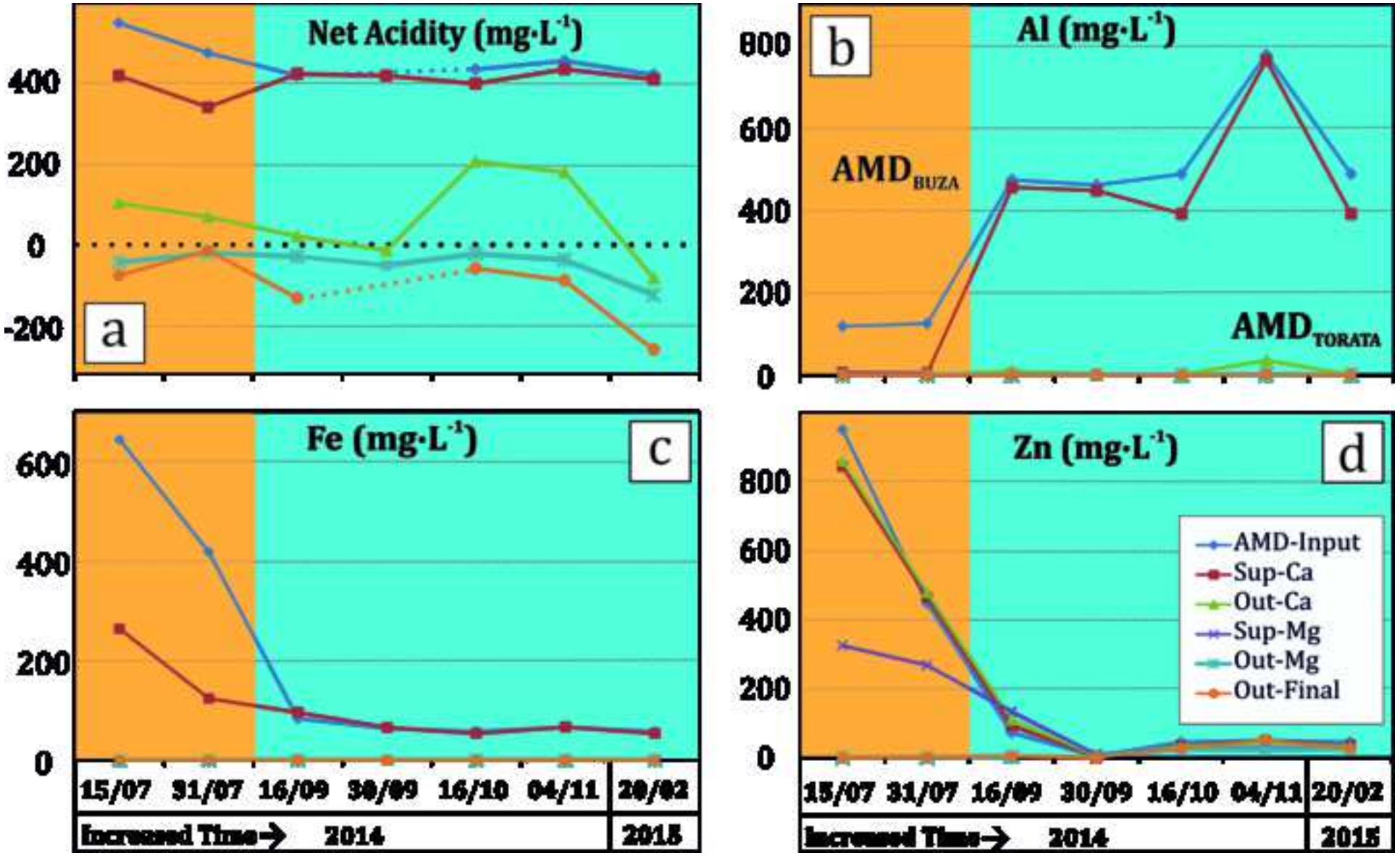

Figure 5-revised

Click here to access/download;Figure;Figure 5.tif

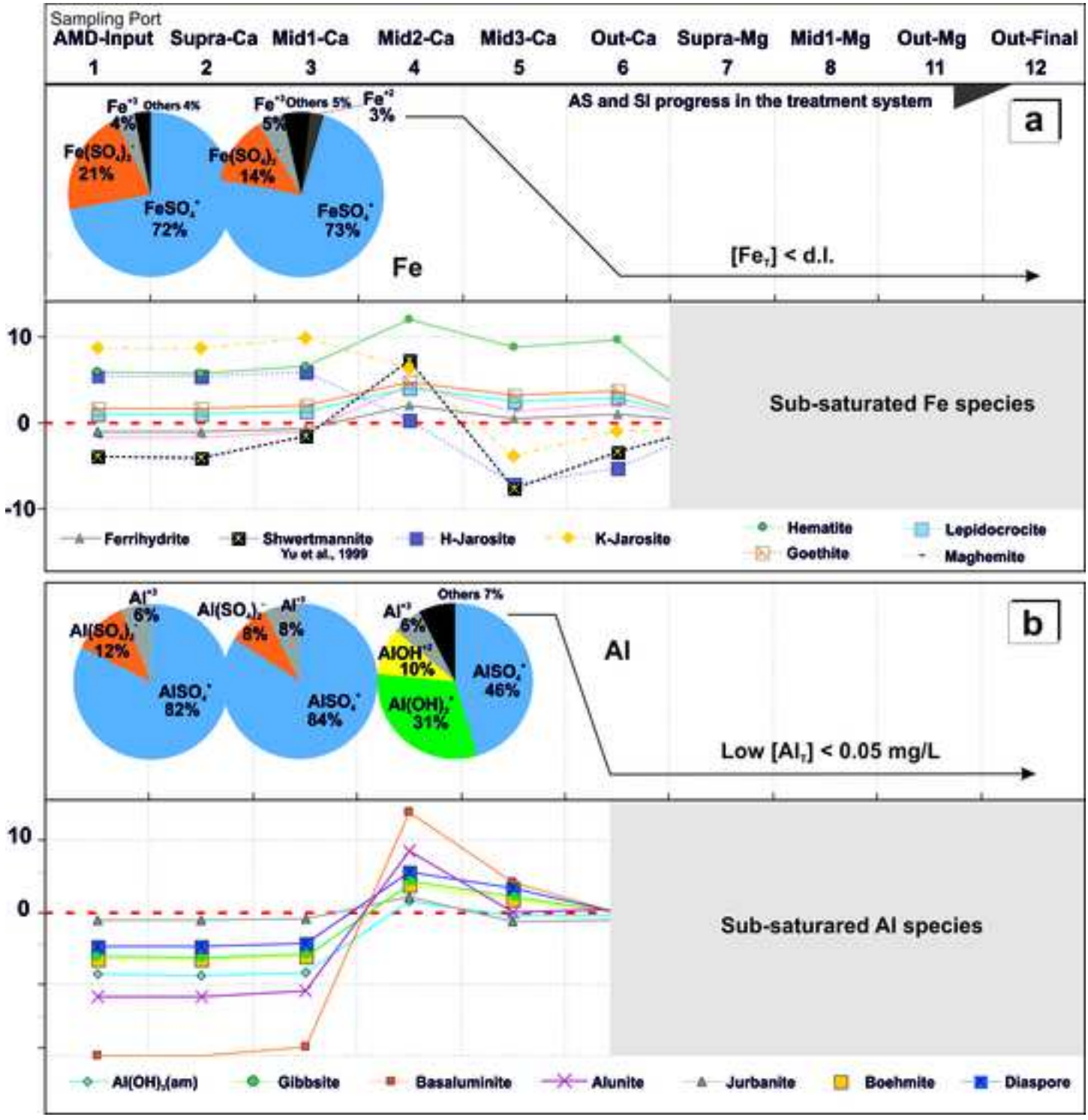

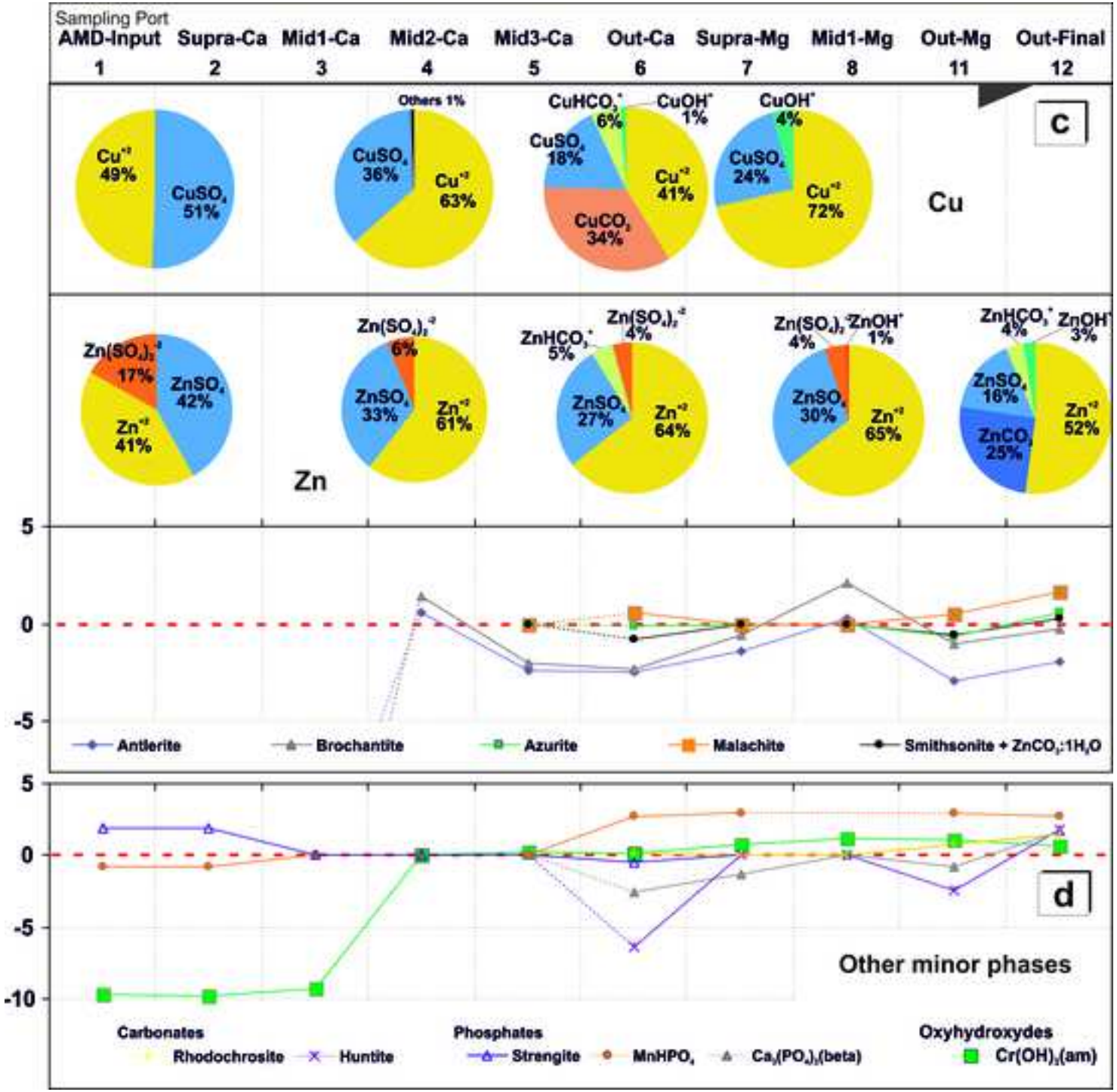

Figure 6-revised

Click here to access/download;Figure;Figure 6.tif

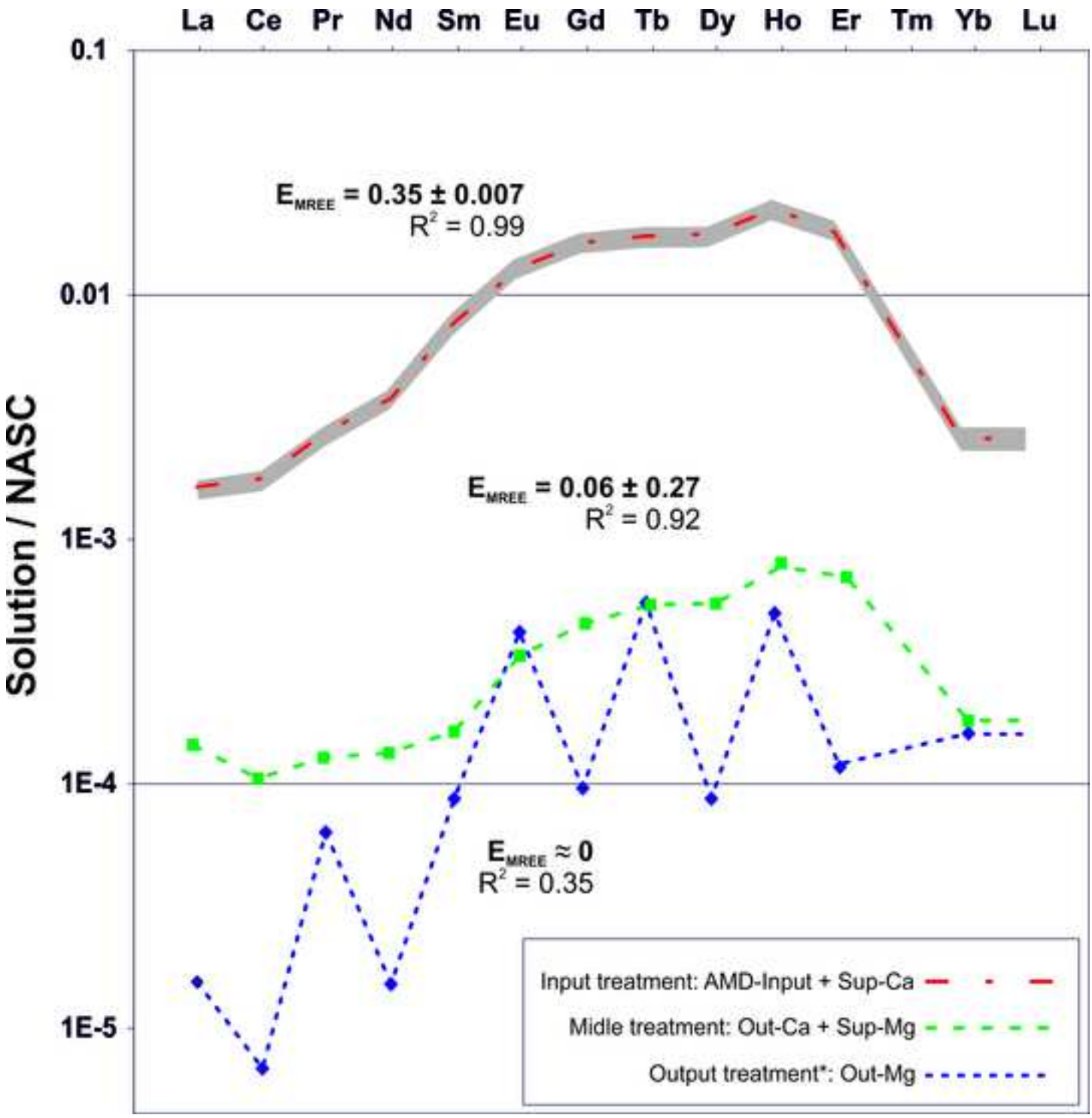

Figure 7-revised

Click here to access/download;Figure;Figure 7.tif

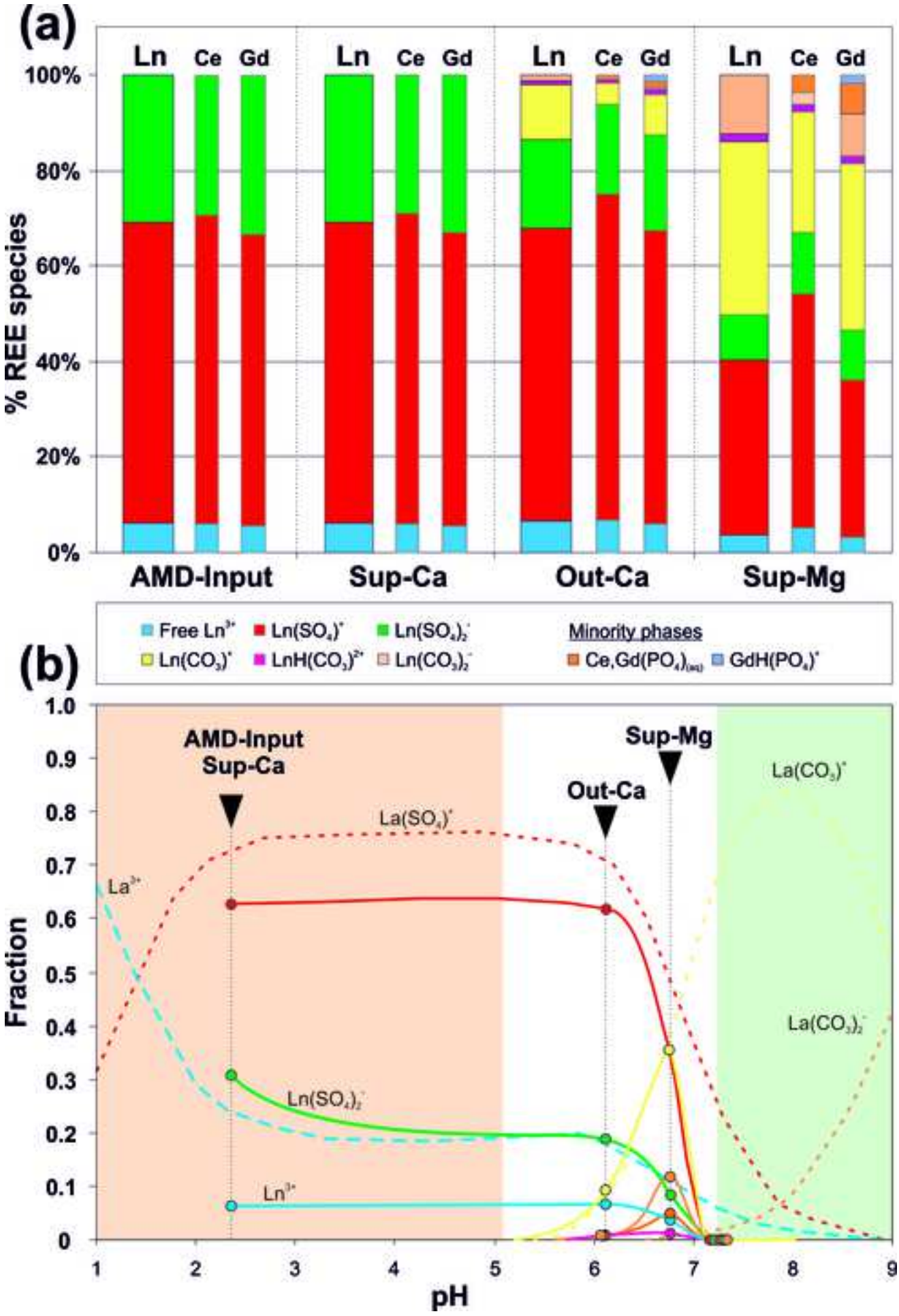

Figure 8-revised

Click here to access/download;Figure;Figure 8.tif

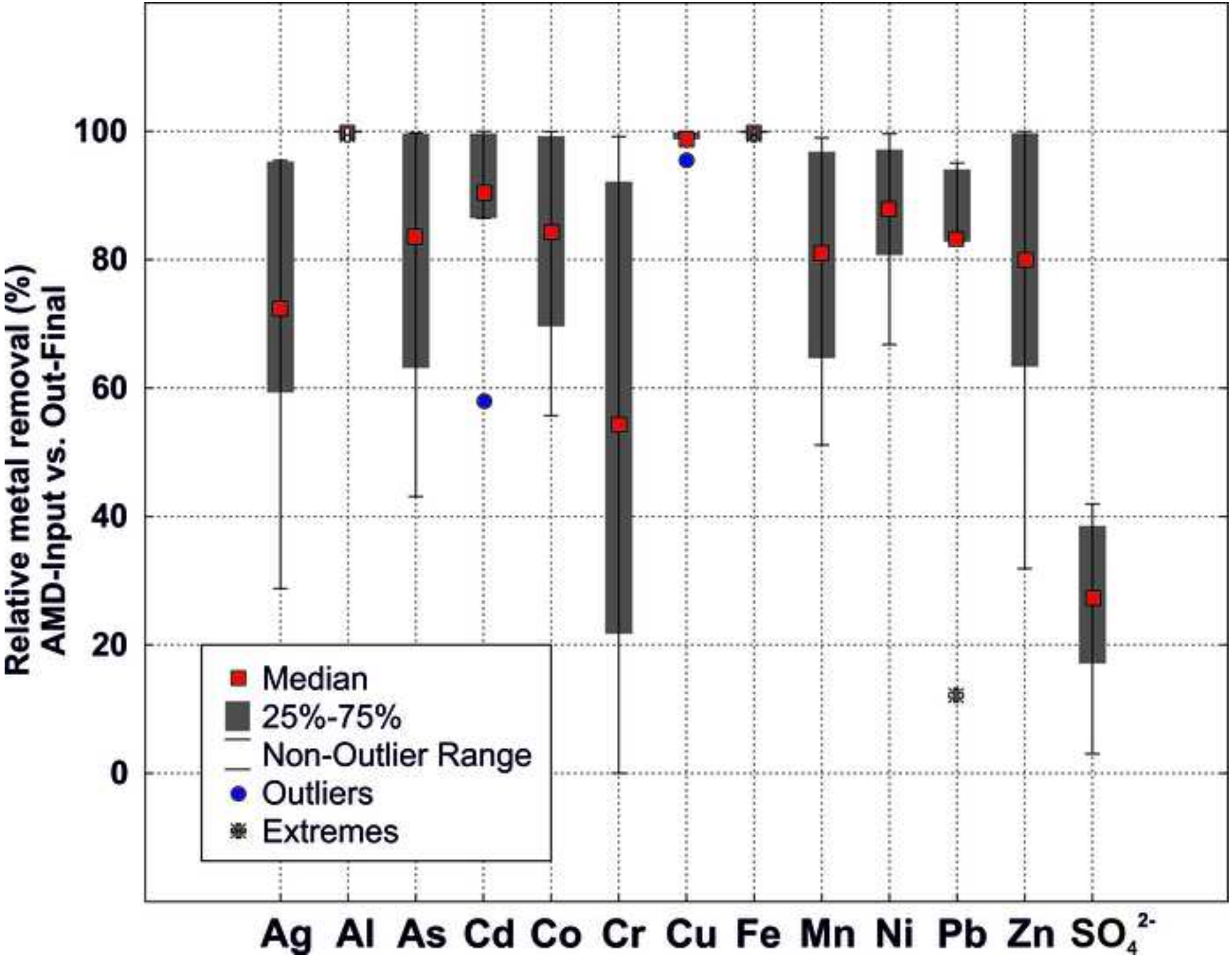

Figure 9-revised

Click here to access/download;Figure;Figure 9.tif

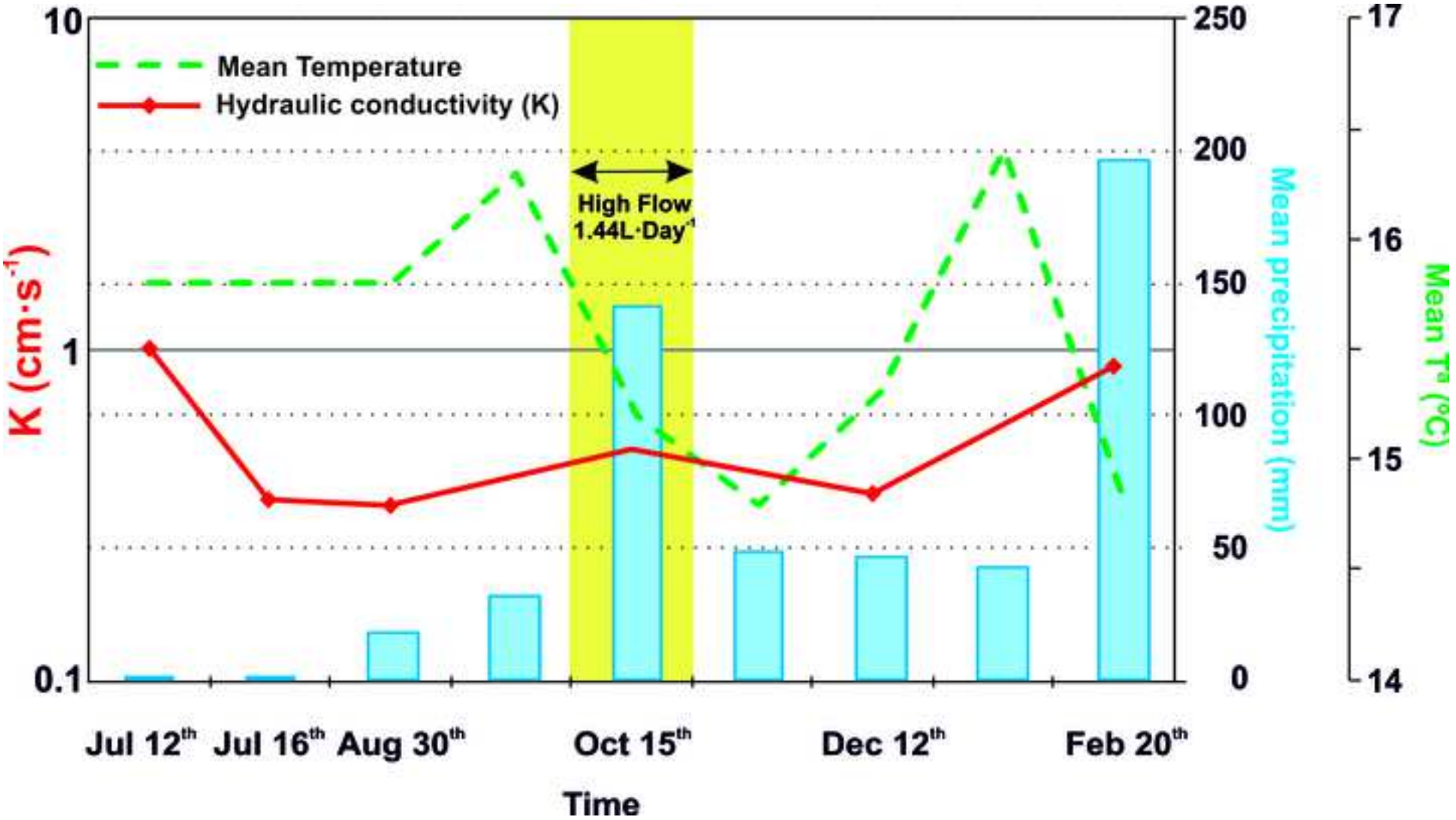

Table 1

Imput source		Code *d.l.*	pH	E.C.	Alk	Acidity	Ag *0,013*	Al *0,02*	As *0,05*	Ca *0,005*	Cd *0,008*	Co *0,005*	Cr *0,018*	Cu *0,043*	Fe *0,005*	Mg *0,005*	Mn *0,019*	Ni *0,017*	Pb *0,044*	Zn *0,17*	SO_4^{2-} *2*
Imput source	Buza/First sampling (15/07/2014)	**AMD-Input**	2,7	4,7	<20	4361	0,02	531	0,07	416	7,03	2,12	0,13	335	121	202	66,8	0,24	0,19	698	4707
		Supra-Ca	4,1	4,1	<20	2200	0,03	194	0,05	999	6,41	2,21	0,06	203	4,98	218	63,2	0,22	0,12	654	3757
		Out-Ca	5,9	3,9	183	973	0,05	1,26	0,05	1128	6,36	2,39	0,05	61,2	0,42	212	68,8	0,28	0,08	668	3212
		Supra-Mg	6,7	4,1	190	283	0,02	0,16	<d.l.	788	2,66	0,99	0,03	16,9	0,13	699	35,8	0,02	0,03	296	3176
		Out-Mg	8,8	4,4	76	-70	<d.l.	0,08	<d.l.	389	0,01	0,01	0,01	0,20	0,17	1114	1,71	0,01	0,02	1,05	3254
		Out-Final	8,1	4,6			0,05	0,09	<d.l.	246	0,01	0,01	0,01	0,19	0,14	1089	1,73	0,01	0,02	0,91	3633
	Torata/First sampling (16/09/2014)	**AMD-Input**	2,5	3,0	20	426	0,01	83,5	2,06	95,1	0,62	1,00	0,01	29,8	474	109	21,3	0,92	0,19	71,7	2934
		Supra-Ca	2,5	2,9	20	429	0,1185	95,6	2,33	122	0,84	1,02	0,01	37,1	456	123	22,7	0,92	0,20	91,7	2108
		Out-Ca	5,8	2,2	190	34,5	<d.l.	0,97	0,10	729	1,26	1,06	0,01	56,5	8,59	120	24,0	0,97	0,08	109	2001
		Supra-Mg	6,0	1,9			<d.l.	0,26	<d.l.	695	1,55	1,09	0,01	33,3	0,60	138	25,4	0,95	0,04	132	1904
		Out-Mg	9,3	3,1			<d.l.	0,01	<d.l.	206	0,04	0,03	0,01	0,73	0,16	431	0,83	0,02	0,02	2,85	1730
		Out-Final	8,5	3,3	190	-116	<d.l.	0,01	0,04	220	0,01	0,08	0,01	0,12	0,14	413	1,86	0,03	0,01	3,88	1733
	Torata/Last sampling (20/02/2015)	**AMD-Input**	2,4	2,6	20	1307	0,21	57,6	12,4	129	0,38	1,23	0,04	13,6	488	134	25,7	1,39	0,17	43,9	3075
		Supra-Ca	2,3	1,9	20	1089	0,12	53,6	4,64	101	0,28	1,10	0,04	10,7	391	107	21,3	1,21	0,34	34,2	2500
		Out-Ca	6,2	1,5	263	-173	0,11	0,01	<d.l.	824	0,30	1,10	0,02	8,56	0,01	117	21,7	1,16	0,01	31,9	2150
		Supra-Mg	6,7	2,1			0,04	0,01	<d.l.	835	0,23	0,91	0,02	6,69	0,01	133	21,4	0,99	0,01	26,5	1950
		Out-Mg	7,1	1,7	255	-188	0,07	0,01	<d.l.	602	0,04	0,76	0,02	1,07	0,01	288	15,9	0,48	0,01	24,5	1825
		Out-Final	8,0	1,6	343	-285	0,09	0,01	<d.l.	494	0,06	0,39	0,02	0,57	0,01	334	9,83	0,28	0,01	25,1	1850
Legal limits		***FAO***	*6.5-8.4*				*n.d.*	*5*	*0,1*	*n.d.*	*0,01*	*0,05*	*0,1*	*0,2*	*5*	*n.d.*	*0,2*	*0,2*	*5*	*2*	*n.d.*
		WHO	*6.5-8.5*		*n.d.*		*n.d.*	*0,9*	*<d.l.*	*n.d.*	*0,003*	*n.d.*	*0,05*	*2*	*2,0*	*n.d.*	*0,4*	*0,07*	*0,01*	*3*	*n.d.*
		TULSMA					*0,1*	*5*	*0,1*	*n.d.*	*0,02*	*0,5*	*0,5*	*1*	*10*	*n.d.*	*2,0*	*2*	*0,2*	*5*	*1000*

E.C.: Electrical conductivity (mS/cm); Alk: Total alkalinity as mg/L of $CaCO_3$; n.d. no data reported; d.l. detection limit; Data expressed in $mg \cdot L^{-1}$

Table 2-Revised

Sampling Port	AMD-Input 1	Supra-Ca 2	Mid1-Ca 3	Mid2-Ca 4	Mid3-Ca 5	Out-Ca 6	Supra-Mg 7	Mid1-Mg 8	Out-Mg 11	Out-Final 12
pH	2,4	2,3	2,4	5,8	6,4	6,3	6,6	7,3	7,0	8,0
Temp (ºC)	21,5	21,5	21,7	21,7	21,7	21,2	21,5	21,7	21,6	21,9
Eh_H (mV)	821	794	772	344	460	507	445	406	465	409
pe	13,9	13,4	13,1	5,82	7,78	8,57	7,52	6,86	7,85	6,91
Alkalinity*	20	n.d.	n.d.	n.d.	n.d.	366	n.d.	n.d.	341	409
Ca	118	125	153	804	1027	873	857	177	602	714
Mg	119	125	140	142	177	162	242	547	394	366
K	3,12	3,17	3,75	3,5	3,65	4,00	3,99	4,57	4,25	4,56
Fe	230	257	259	6,82	<d.l.	0,02	<d.l.	0,02	0,02	0,01
Mn	26,3	27,9	31,1	30,0	31,7	27,5	28,0	6,47	19,0	9,64
Cr	0,06	0,05	0,07	0,03	0,02	0,03	0,03	0,01	0,02	0,02
Co	1,54	1,54	1,61	1,67	1,18	1,40	1,24	0,11	0,66	0,61
S(6)**	4535	4579	3177	2454	1959	1842	1567	1900	2088	1512
P***	7,3	7,9	n.d.	n.d.	n.d.	0,90	0,90	n.d.	0,90	1,00
Ag	0,2	0,25	0,22	0,07	0,12	0,07	0,18	0,05	0,10	0,20
Al	61,2	64,3	72,4	58,6	0,08	0,08	0,09	0,06	0,08	0,09
As	7,05	7,50	4,18	0,03	0,06	0,03	0,04	0,01	0,02	0,03
Cd	0,40	0,41	0,39	0,33	0,15	0,19	0,21	0,11	0,07	<d.l.
Cu	16,0	16,1	17,8	33,1	0,54	1,32	0,56	0,28	0,22	0,24
Ni	1,72	1,71	1,81	1,87	1,25	1,45	1,33	0,09	0,56	0,68
Pb	0,74	0,22	0,19	0,13	<d.l.	0,01	<d.l.	<d.l.	<d.l.	<d.l.
Zn	46,8	48,8	55,0	52,0	13,4	12,5	13,7	7,02	3,90	3,05

Concetrations are expressed in $mg{\cdot}L^{-1}$ (* Alcalnity as HCO_3^- ** S(6) as SO_4^{-2} *** P as PO_4^{-3}) / n.d. not determined; <d.l. below detection limit Calculations based on the Oxidation-reduction potential: $Eh_H(mV)=Ehpl(mV) + 223.8 - 1.02*t(ºC)$; $pe=16.9*(Eh_H/1000)$

Table 3-Revised

Solution	AMD-Input	Supra-Ca	Out-Ca	Supra-Mg	Out-Mg	Out-Final		
Elements							**unit**	**type of input value**
La	5,30E-02	5,13E-02	6,45E-03	4,04E-03	< d.l.	< d.l.	$mg{\cdot}L^{-1}$	total concentration
Ce	1,32E-01	1,27E-01	9,77E-03	5,88E-03	< d.l.	< d.l.	$mg{\cdot}L^{-1}$	total concentration
Pr	2,19E-02	2,12E-02	2,41E-03	7,59E-04	< d.l.	< d.l.	$mg{\cdot}L^{-1}$	total concentration
Nd	1,28E-01	1,23E-01	1,16E-02	3,73E-03	< d.l.	< d.l.	$mg{\cdot}L^{-1}$	total concentration
Sm	4,52E-02	4,35E-02	2,28E-03	7,88E-04	< d.l.	< d.l.	$mg{\cdot}L^{-1}$	total concentration
Eu	1,58E-02	1,53E-02	9,15E-04	< d.l.	< d.l.	< d.l.	$mg{\cdot}L^{-1}$	total concentration
Gd	8,80E-02	8,46E-02	9,26E-03	2,92E-03	< d.l.	< d.l.	$mg{\cdot}L^{-1}$	total concentration
Tb	1,60E-02	1,54E-02	1,72E-03	6,94E-04	< d.l.	< d.l.	$mg{\cdot}L^{-1}$	total concentration
Dy	1,04E-01	1,00E-01	7,12E-03	4,08E-03	< d.l.	< d.l.	$mg{\cdot}L^{-1}$	total concentration
Ho	2,30E-02	2,21E-02	3,65E-03	1,09E-03	< d.l.	< d.l.	$mg{\cdot}L^{-1}$	total concentration
Er	6,46E-02	6,22E-02	5,89E-03	3,23E-03	< d.l.	< d.l.	$mg{\cdot}L^{-1}$	total concentration
Tm	8,42E-03	8,12E-03	1,25E-03	< d.l.	< d.l.	< d.l.	$mg{\cdot}L^{-1}$	total concentration
Yb	4,80E-02	4,64E-02	5,42E-03	< d.l.	< d.l.	< d.l.	$mg{\cdot}L^{-1}$	total concentration
Lu	7,03E-03	6,79E-03	8,00E-04	< d.l.	< d.l.	< d.l.	$mg{\cdot}L^{-1}$	total concentration
Ligands								
PO_4^{3-}	7,90E+00	9,25E+00	8,50E-01	1,00E+00	1,05E+00	9,50E-01	$mg{\cdot}L^{-1}$	total concentration
SO_4^{2-}	4,53E+03	4,47E+03	1,91E+03	1,75E+03	1,96E+03	1,89E+03	$mg{\cdot}L^{-1}$	total concentration
CO_3^{2-}	1,20E+01	1,20E+01	1,80E+02	1,74E+02	1,68E+02	2,01E+02	$mg{\cdot}L^{-1}$	total concentration
Parameters								
Alkalinity	20	20	300	290	280	335	$mg{\cdot}L^{-1}$ *	total concentration
pH	2,4	2,3	6,2	6,7	7,1	8,0		-
pe	13,71	13,19	8,57	8,32	8,25	7,23		-

* Alkalinity as $mg{\cdot}L^{-1}$ for HCO^{3-} / < d.l. below detection limit.

Calculations based on the Oxidation-reduction potential: $Eh_H(mV)=Eh_{pl}(mV) + 223.8 - 1.02*t(ºC)$; $pe=16.9*(Eh_H/1000)$

Table 4

Total Recovery Treatment	240 days					
	Flow: 1 month at 0,66 L/Day and 7 month 1,44 L/day					
Basic metal	**Al**	**Cu**	**Fe**	**Mn**	**Zn**	**∑REE**
Concentration (mg/L)	64,7	16,8	796	57,6	19,4	0,754
gr (8 month)	20,2	6,49	18,8	8,18	13,3	0,11

Total Simulation	1 year					
	Flow: 1 L/s (Torata mine shaft mean annual value)					
mg/day	55832587	28916585	10455996	60239287	1280413	65146
Total recovery (Kg/yr)	20379	10555	3816	21987	467	24
Tons/yr	**20**	**11**	**3,8**	**22**	**0,5**	**0,024**